applied sciences

MDPI

Article

Short-Session GNSS Monitoring of Normal Heights Above Underground Mine Workings: Optimisation of a Multi-Reference Configuration and Inter-Cycle Comparison with Precise Levelling

Guldana Meirambek [1], Zhandos Shakirov [1], Emil Bayramov [2], Kanay Rysbekov [1], Marzhan Nurpeissova [1], Dinara Kirgizbaeva [1,*], Saule Soltabayeva [1], Shynar Aitkazinova [1], Gulmira Madimarova [1] and Alima Nurzhussupova [1]

[1] Department of Surveying and Geodesy, O.A. Baikonurov Mining and Metallurgical Institute, Kazakh National Research Technical University Named After K.I. Satbayev, 22 Satbayev Street., Almaty 050013, Kazakhstan; g.meirambek@satbayev.university (G.M.); shakirov.zha@gmail.com (Z.S.); k.rysbekov@satbayev.university (K.R.); m.nurpeissova@satbayev.university (M.N.); s.soltabayeva@satbayev.university (S.S.); sh.aitkazinova@satbayev.university (S.A.); g.madimarova@satbayev.university (G.M.); nurzhusupovaalima@gmail.com (A.N.)

[2] School of Engineering, Department of Mining and Geosciences, Nazarbayev University, 53 Kabanbay Batyr Avenue, Astana 010000, Kazakhstan; emil.bayramov@nu.edu.kz

* Correspondence: mejrambekovnadinara@gmail.com

Featured Application

The validated three-reference, 60 min static GNSS configuration can support operational monitoring of normal-height changes above underground mine workings between periodic campaigns of high-precision geometric leveling.

Abstract

Reliable monitoring of an underground mining area requires separating movement of the monitored surface from instability of the reference frame while maintaining the feasibility of observations within short field windows. At a monitoring site covering approximately 2.2 km^2, twelve monitoring benchmarks are located above the surface projections of mapped mine-working corridors, while Burovaya, Poselkovyi, and 5784 form an external triangular reference subnetwork; Burovaya was adopted as the primary point, and the coordinates of the two secondary stations are re-determined in each cycle. Five cycles of dual-frequency global navigation satellite system (GNSS) observations were conducted using the Global Positioning System (GPS), the Global Navigation Satellite System (GLONASS), and Galileo jointly. The same rover records were reprocessed under nine conditions: one, two, and three reference stations with nested intervals of 15, 30, and 60 min. Ellipsoidal heights were converted to normal heights in the Baltic height reference frame using a local transformation with a planar approximation of the height component, without applying a geoid or quasigeoid model. Interferometric synthetic aperture radar (InSAR) data from 21 Sentinel-1C epochs spanning 26 May 2025 to 2 June 2026 were used for the spatio-temporal characterisation of the reference configuration; a relative line-of-sight (LOS) velocity of +0.0 ± 1.9 mm/year (formal 1σ) was obtained for Burovaya; its magnitude was smaller than the quoted formal uncertainty and was not statistically significant. This result supports the relative stability of the station within the sensitivity of the method and the observation period. Precise geometric levelling was performed in Cycles 3–5; external evaluation was conducted at Rp-1…Rp-12.

Academic Editors: Robert Tenzer and Mehdi Eshagh

Received: 11 September 2026
Revised: 5 November 2026
Accepted: 8 November 2026
Published: 12 November 2026

Copyright: © 2026 by the authors. Licensee MDPI, Basel, Switzerland. This article is an open access article distributed under the terms and conditions of the Creative Commons Attribution (CC BY) license.

The cycle-specific root mean square difference (RMSE) values for the 'three reference stations, 60 min' mode were 4.6, 3.5, and 2.4 mm for Cycles 3, 4, and 5, respectively. For the 3→4 and 4→5 transitions, GNSS and levelling indicated the same direction of change at all 12 benchmarks. Paired analysis of Cycles 3–5 at 60 min confirmed the advantage of the tested three-reference configuration over the one- and two-reference configurations, whereas the advantage of 60 min over 30 min was small and statistically non-significant. Therefore, 60 min is regarded as a practical and robust working interval among those tested, rather than as a statistically demonstrated optimum.

Keywords: GNSS; static observations; geodynamic monitoring site; InSAR; normal height; precise geometric levelling; short baselines; deformation monitoring

1. Introduction

Safe operation of deposits involving underground mining requires reproducible monitoring of small vertical changes in the ground surface. The reliability of such monitoring depends on the stability of the reference frame, the reproducibility of global navigation satellite system (GNSS) antenna installation, the correctness of the local transformation, and the observation conditions. In this study, the influence of these factors was reduced through spatially justified placement of the reference stations, forced antenna centring, the use of short baselines, a local transformation with a planar approximation of the height component, and external comparison with precise levelling at benchmarks not involved in establishing the transformation. Therefore, the accuracy of the proposed scheme was evaluated not only by the formal indicators of the GNSS solutions but also by its actual agreement with the precise levelling results.

Precise geometric levelling remains the most reliable terrestrial method for transferring normal heights, but it also has instrumental, staff-related, refraction-related, setup, and network uncertainties. Repeated long levelling routes require stable installation of the tripod and staffs, intervisibility, and favourable refraction conditions. Strong winds and persistent snow cover substantially increase labour requirements and the risk of impaired reproducibility; levelling control was absent in Cycles 1–2 because of a combination of field and organisational factors, and only Cycle 2 was conducted in winter. This creates a practical need for a GNSS protocol capable of supporting monitoring between full levelling campaigns, without treating levelling as an error-free reference or as a method that can be completely replaced.

Static GNSS positioning does not require intervisibility between points and enables more rapid coverage of a spatially distributed network. However, the vertical component is sensitive to satellite geometry, residual tropospheric delay, multipath, the antenna phase-centre model, and session duration [1–5]. Published recommendations differ because of variations in baseline lengths, monumentation types, height systems, and accuracy criteria [1–3,6–9]. Therefore, a one-hour session cannot be justified by a general rule; it must be verified specifically for the short baselines, forced centring, and local datum of the study site.

Interferometric synthetic aperture radar (InSAR), GNSS, precise levelling, and other external measurements have already been jointly applied in integrated monitoring systems [10–16]. InSAR provides a spatially dense signal along the satellite line of sight (LOS) and can support the selection of GNSS station locations [17–19], but a single-direction LOS measurement cannot be regarded as vertical displacement without geometric decomposition.

For the subsequent spatio-temporal characterisation of the reference configuration

already selected, InSAR data for the available later period and the underground mine-workings plan were analysed. Burovaya, the primary reference station, is located outside the surface projection of the underground mine workings. Poselkovyi and 5784 are also located outside this projection. Their coordinates were re-determined in each cycle relative to Burovaya as an independent precaution against possible reference changes; this procedure was not introduced as a consequence of the later InSAR assessment.

Individual elements of the proposed approach are established: multi-baseline and multi-reference GNSS networks, shortened static sessions, InSAR-supported design, and levelling control [1–4,6–9,14–20]. Their combined application in a compact network remains insufficiently studied where (i) the external reference subnetwork is spatially separated from the surface projection of the mapped underground mine workings; (ii) the monitoring benchmarks are located above mapped mine-working corridors; (iii) the same rover records permit paired comparisons of 1/2/3 reference points and 15/30/60 min; (iv) GNSS results are converted to local normal heights; (v) the mode is selected from three separate field cycles with levelling control, rather than from a single demonstration epoch; and (vi) suitability for monitoring is evaluated separately using absolute heights and inter-cycle changes. The scientific novelty of this work lies in the experimental substantiation and repeated field validation of an operational mode for local GNSS monitoring of vertical ground-surface changes above underground mining areas. Across five cycles, the same rover records were used to compare nine combinations of three predefined nested reference configurations—Burovaya; Burovaya + Poselkovyi; Burovaya + Poselkovyi+5784—and static observation durations of 15, 30, and 60 min. In Cycles 3–5, an external comparison of normal heights with precise levelling results was performed for each configuration at 12 control benchmarks that were not used to fit the transformation. This experimental design enabled comparison of the specific reference configurations and observation durations and selection of a practical site-specific mode with three reference stations and 60 min sessions for the compact network investigated. The methodology was supplemented by placing the reference stations outside the underground mine workings, spatio-temporal characterisation of the reference configuration using InSAR data, and a local transformation with a planar approximation of the height component.

At the local scale, the integration of GNSS, precise levelling, and InSAR within the proposed workflow supports Earth system monitoring by providing repeatable observations of surface-height changes in an area affected by underground mining.

The aim of the study was to select and evaluate over multiple campaigns a site-specific configuration for short-session GNSS monitoring of normal heights above underground mine workings. Three questions were examined: how the specific composition of the reference configuration and the duration affect GNSS agreement with precise levelling; whether the full three-reference configuration retains its advantage in Cycles 3–5; and how similar the route profiles of inter-cycle dynamics obtained by the two methods are. The principal external indicators were the mean signed difference (MD), standard deviation of the differences (SD), mean absolute difference (MAE), root mean square difference (RMSE), and maximum absolute difference at Rp-1…Rp-12, which were excluded from determination of the height transformation. The dynamics were analysed separately as ΔH_{GNSS} and ΔH_{lev} relative to a common reference epoch; the diagnostic discrepancy between these estimates was not interpreted as the error of either method.

2. Materials and Methods

This section describes, in sequence, the spatial organisation of the network, the role of InSAR, the field observation cycles, GNSS processing, the local transformation, pre-

cise levelling, and the statistical framework for external comparison.

2.1. Study Site and Spatial Structure of the Network

The study was conducted at the technogenic geodynamic monitoring site of the Vostochnaya-Saryoba deposit in the Ulytau Region, Republic of Kazakhstan. The monitored area is approximately 2.2 km^2. The geodetic network comprises two groups of points with different functions. The reference subnetwork consists of Burovaya, Poselkovyi, and 5784, which are located outside the surface projection of the underground mine workings. The monitoring subnetwork comprises benchmarks Rp-1…Rp-12, located within the monitored area above sections of the underground mine workings.

The monitoring subnetwork comprises twelve monitoring benchmarks, Rp-1…Rp-12. They are located above the surface projections of mapped mine-working corridors and are intended to record spatially differentiated vertical changes directly above the mined area. This placement provides targeted monitoring of vertical dynamics within zones potentially affected by underground mining and enables the spatial distribution of the detected changes to be compared with the location of the mine workings. Rp-1…Rp-6 are existing metal benchmarks; Rp-7…Rp-12 were installed as part of the project. In the primary analysis, both groups are considered jointly without assigning different reliability a priori.

The reference subnetwork consists of Burovaya, Poselkovyi, and 5784, which form a triangle enclosing the site area. According to the available plan, they are located outside the surface projection of the depicted underground mine workings. Burovaya was adopted as the primary datum point. The coordinates of Poselkovyi and 5784 were redetermined in each cycle within a hierarchy originating from Burovaya, after which these points were used as secondary reference stations. The maximum reference-to-rover baseline did not exceed 3.7 km. The spatial classification was based on a combined examination of the overview diagram and the mine-workings plan revised in October 2024. The overview configuration of the network is shown in Figure 1, and the positions of the benchmarks relative to the underground mine-working corridors are shown in Figure 2.

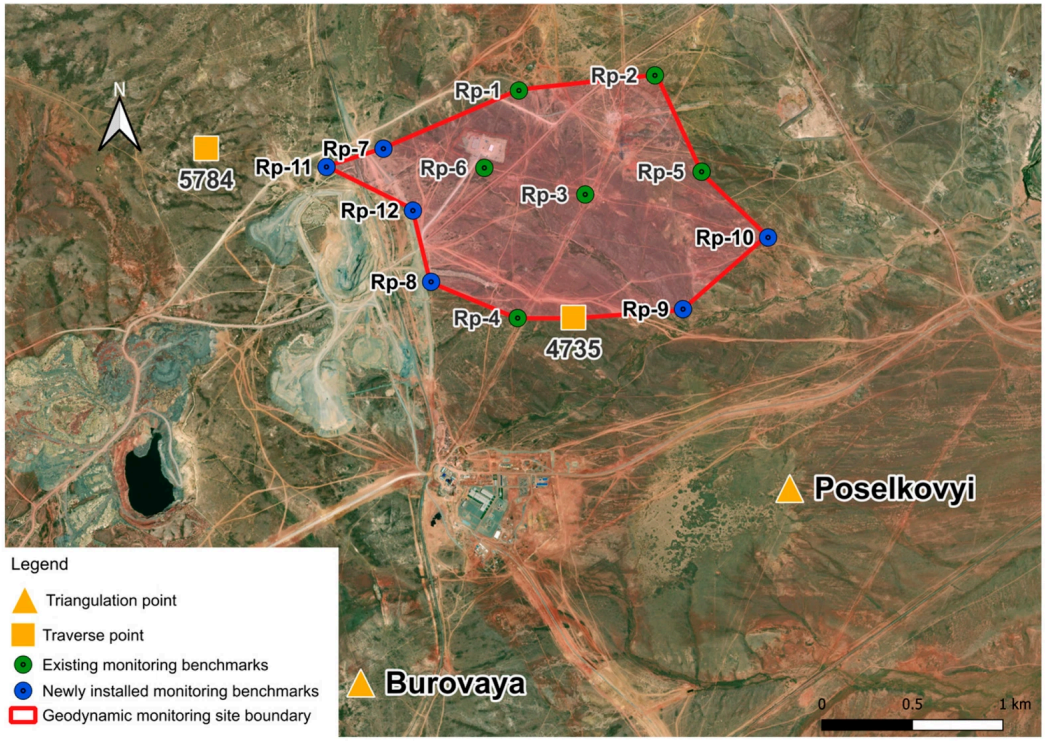
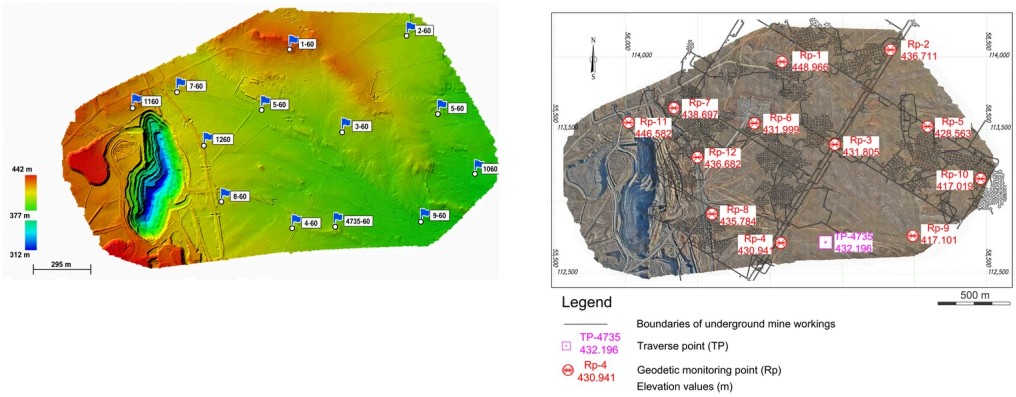


Figure 1. Overview diagram of the external reference subnetwork and the monitored site. Burovaya, Poselkovyi, and 5784 are located outside the surface projection of the mapped underground mine workings.



(a) **(b)**

Figure 2. Spatial basis for network design: (**a**) digital elevation model of the study area showing the monitoring points; (**b**) orthophotomosaic showing the monitoring benchmarks Rp-1…Rp-12 and the surface projections of the mapped underground mine-working corridors.

The authors' digital elevation model and orthophotomosaic were used as the cartographic base for network design and for comparing the positions of the benchmarks with the terrain and the surface projections of the underground mine workings. These materials provided the spatial basis for point placement and were not used as independent evidence of deformation.

2.2. Spatio-Temporal Characterisation of the Reference Configuration Using InSAR Data

MintPy [21–23] was used for persistent-scatterer time-series analysis. In this study, InSAR was used only to compare relative LOS velocities near the geodetic points; absolute surface velocities and GNSS normal-height changes were not derived from these

data. The set of 24 original Sentinel-1C C-band images comprised all data available for the selected area and acquisition geometry. The images were acquired in Interferometric Wide (IW) swath mode on descending relative orbit 49 with vertical-transmit/vertical-receive (VV) polarisation between 20 April 2025 and 2 June 2026; three early images were excluded. The analysis retained 21 epochs spanning 26 May 2025 to 2 June 2026 (372 days). The historical MintPy version used in the original processing was not recorded in the processing materials; version 1.6.4 is cited only as a publicly available release checked when preparing the response to the reviewer, and no equivalent reprocessing is claimed.

The three excluded acquisitions were dated 20 April, 2 May, and 14 May 2025. Geocoded coordinates were expressed in WGS 84 (EPSG:4326), and displacement was referenced to the first retained epoch.

The topographic phase component was removed using the SRTM-3 v4 digital elevation model. The network comprised 79 accepted interferometric pairs with temporal baselines of 12–180 days; all 21 epochs formed a single connected network. Goldstein filtering, minimum-cost-flow phase unwrapping on a Delaunay network, and atmospheric phase-screen estimation were applied. The coherence threshold used during phase unwrapping was 0.30.

Connection selection used temporal separations of 0–180 days, normal baselines of 0–2% of the critical baseline, minimum-normal-baseline selection, low redundancy, and a nominal limit of eight links per image. The 79 accepted unique pairs formed one connected network with 4–10 links per image (mean 7.524); absolute normal baselines ranged from 1.949 to 108.455 m. The super-reference acquisition was 11 September 2025, which is distinct from the exported temporal origin and the spatial displacement datum.

Coregistration and interferogram generation used four range looks and one azimuth look with spectral-shift filtering. Goldstein filtering used a 64-pixel window, 80% overlap, and alpha limits of 0.30–2.50; coherence was estimated over a 5 × 5 window. Both unwrapping stages used minimum-cost flow on a Delaunay network. Inversion used weighted Jacobi singular-value decomposition, linear displacement models, and residual-height estimation. Atmospheric filtering used a 1600 m spatial low-pass window and a 365-day temporal high-pass window. Layover/shadow masking and automatic refinement were enabled.

The geocoded sample comprised 94,908 persistent scatterers. The following export criteria were applied: temporal coherence of at least 0.1 (a threshold used only to select exported results, not the phase-unwrapping threshold), formal velocity uncertainty not exceeding 8 mm/year, and height uncertainty not exceeding 10 m. For Burovaya, 5784, Poselkovyi, and 4735, the nearest retained scatterers were located 4.1–6.4 m from the geodetic points; their temporal coherence values were 0.913, 0.911, 0.909, and 0.840, respectively. These values characterise nearby reflecting targets rather than direct radar measurements of the geodetic monument centres themselves.

The spatial extent of the retained persistent-scatterer sample was defined by its outer convex envelope (48.127594–48.171130° N; 67.440867–67.502556° E), which covers approximately 18.1 km^2 around the 2.2 km^2 GNSS monitoring site. The envelope defines the extent of the retained sample and does not imply continuous measurement coverage; it is distinct from the displacement reference area and the mapped mine-working boundaries. All four stations in Table 1 lie within this envelope. Rp-2 lies near its northern edge and is represented by a persistent scatterer approximately 3.4 m away.

Table 1. Relative LOS velocities and formal 1σ uncertainties for the persistent scatterers nearest to the points; the values retain the original InSAR spatial datum.

Point	Latitude	Longitude	LOS Velocity ± 1σ, mm/Year	Role in the GNSS Configuration	Coherence
Burovaya	48°08′12.72707″ N	67°27′41.60419″ E	+0.0 ± 1.9	Primary datum point	0.913
5784	48°09′48.06827″ N	67°27′00.26513″ E	+0.6 ± 1.7	Secondary reference station, re-determined in each cycle	0.911
Poselkovyi	48°08′47.43531″ N	67°29′36.25544″ E	+1.7 ± 2.0	Secondary reference station, re-determined in each cycle	0.909
4735	48°09′17.91344″ N	67°28′38.42789″ E	−2.1 ± 2.1	Local transformation point, not included in the validation dataset	0.840

The retained persistent scatterers had temporal coherence of 0.101–0.977, formal velocity uncertainty of 0.3–5.8 mm/year, and height uncertainty of 0.976–9.994 m. Valid-interferogram percentages ranged from 65.823% to 100%, corresponding to 52–79 valid equations, and 88,495 scatterers retained all 79 accepted pairs. At the four station-associated scatterers, all 21 acquisitions and all 79 interferometric pairs were valid, the disconnection counter was zero, and the LOS incidence angles ranged from 43.513° to 43.701°.

The original InSAR spatial reference area was selected within a high-coherence zone; its exact historical location was not recorded in the preserved materials. The point with the highest temporal coherence in the retained export (48.152900° N, 67.484980° E; 0.977) is regarded as the most likely candidate for this area. The results are therefore interpreted as relative LOS velocities in the original spatial datum. Positive values denote movement towards the satellite and negative values movement away from it; a single descending geometry does not permit separation of the vertical and horizontal components. The formal 1σ uncertainty was derived from the standard deviations of the persistent-scatterer velocities and does not include possible movement of the reference area, spatially correlated atmospheric residuals, or the offset between the scatterer and the geodetic point. The uncertainty of the LOS-velocity difference between two points also depends on their covariance; because the inter-point covariance was not retained, a separate confidence interval for such a difference was not calculated.

Relative to Burovaya, the LOS-velocity differences were +0.6 mm/year for 5784, +1.7 mm/year for Poselkovyi, and −2.1 mm/year for 4735. Because the inter-scatterer covariance was unavailable, formal standard deviations of these differences could not be determined uniquely. Their conservative upper bounds, obtained as the sums of the corresponding individual formal standard deviations, were 3.7, 3.9, and 4.0 mm/year, respectively. These values bound only the formal component and are not complete error estimates or confidence intervals.

The InSAR period does not cover the first three GNSS cycles. Cycles 4 and 5 fall

within the overall SAR interval but do not coincide with the dates of the retained epochs. The InSAR results are therefore considered in the spatio-temporal characterisation of the reference configuration over the available period. The primary geodetic assessment is based on GNSS observations and precise levelling. The relative LOS velocities and their formal uncertainties are presented in Table 1. The magnitude of each of the four station-associated LOS velocities was smaller than its corresponding 1σ formal uncertainty; therefore, none of the resulting LOS-velocity estimates was statistically significant. These results support the relative stability of the stations within the sensitivity of the method and the observation period. These InSAR results were treated only as supplementary spatio-temporal context and not as validation of the GNSS-derived normal-height changes.

The 20 intervals between successive retained epochs comprised eighteen 12-day intervals, one 24-day interval (3–27 April 2026), and one 132-day interval (10 November 2025–22 March 2026); the retained series therefore does not establish continuous winter behaviour. Cycles 4 and 5 were bracketed by the retained SAR acquisitions of 13 and 25 July 2025 and of 27 April and 9 May 2026, respectively. Accordingly, the InSAR results provide a subsequent consistency check over the observed SAR interval and cannot establish reference-station stability over the entire GNSS campaign or validate GNSS normal-height changes.

The location of Burovaya outside the surface projection of the mapped underground mine workings was the primary spatial condition for its inclusion in the reference configuration. The magnitude of the later relative LOS velocity of the nearest persistent scatterer, +0.0 ± 1.9 mm/year, was smaller than its corresponding formal 1σ uncertainty and was not statistically significant. This result supports the relative stability of Burovaya within the sensitivity of the method and the observation period and was considered as supplementary spatio-temporal context for the available period.

2.3. Monumentation of the Monitored Points

The existing benchmarks Rp-1…Rp-6 are also equipped with forced-centring mechanisms for the GNSS antenna. The existing and new benchmarks differ primarily in embedment depth and in the design of the levelling mark. For Rp-7…Rp-12, a purpose-designed monument with an embedment depth of 3.2 m and an above-ground section 1.0 m high was used. The upper assembly is equipped with a 5/8″ thread for forced centring of the GNSS antenna, while a separate levelling mark is located at a fixed level approximately 0.3 m from the ground surface. This separation reduces the uncertainty of repeated antenna installation and allows the GNSS solution to be linked to the normal height of a separate mark. The developed “Permanent Forced-Centring Point” design is protected by Republic of Kazakhstan Utility Model Patent No. 10736, dated 20 June 2025. The patent holder is K. I. Satbayev Kazakh National Research Technical University (https://repository.satbayev.university/publication/b6d9b476-42ff-435b-acf5-c701e34fd923, accessed on 7 November 2026). According to the KazNRTU repository, the patent status is “Active”, with protection valid until 18 March 2027. The design is regarded as a means of improving reproducibility rather than as the principal scientific novelty of the article; its construction is shown in Figure 3.

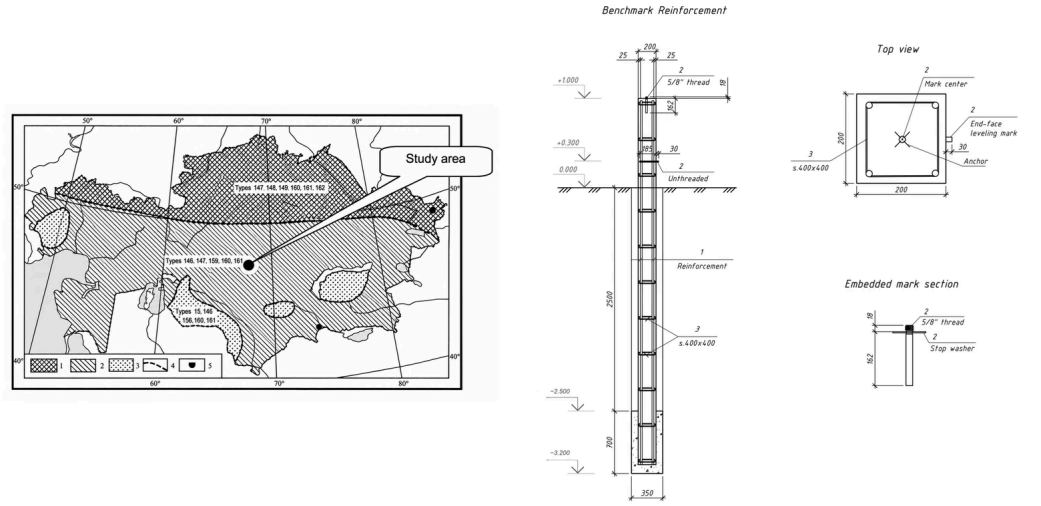


Figure 3. Rationale for the monitoring benchmark design: (**a**) location of the study site within the zone of seasonal ground freezing according to the monument-type application scheme; (**b**) monument design with an embedment depth of 3.2 m, forced centring of the GNSS antenna, and a separate levelling mark.

The embedment depth was calculated using mean monthly negative temperatures from SP RK 2.04-01-2017, 'Construction Climatology' [24]. The sum of the absolute values of the negative mean monthly temperatures, M_t, was 45.2 °C. Taking into account the heterogeneous soil profile, the calculated depth of penetration of the zero isotherm was 2.185 m. The anchor section of the monument was placed 1.0 m below this level; after rounding, the design embedment depth was 3.2 m below the ground surface. This embedment reduces the effects of seasonal freezing and frost heave on monument stability.

2.4. Observation Cycles and Availability of Control

Five cycles of static GNSS observations were performed. In each cycle, the results were processed using nine experimental configurations comprising one, two, and three reference stations with observation durations of 15, 30, and 60 min. In Cycles 3–5, precise geometric levelling was additionally performed, and its results were used for external comparison with the normal heights obtained by GNSS. Only GNSS observations were performed in Cycles 1–2. The dates of the cycles and the measurements performed are presented in Table 2.

Table 2. Observation cycles and status of external levelling control.

Cycle	GNSS Period	GNSS	Levelling	Use in the Analysis
1	16–18.10.2024	Yes	No	Descriptive GNSS dynamics
2	19–21.01.2025	Yes	No	Descriptive GNSS dynamics without seasonal interpretation
3	25–27.04.2025	Yes	Yes (24–27.04.2025)	External evaluation of nine

Cycle	GNSS Period	GNSS	Levelling	Use in the Analysis
				configurations and inter-cycle comparison
4	20–21.07.2025	Yes	Yes (17–20.07.2025)	External evaluation of nine configurations and inter-cycle comparison
5	03–04.05.2026	Yes	Yes (01–03.05.2026)	External evaluation of nine configurations and inter-cycle comparison

Inter-cycle dynamics of normal heights were evaluated using the results of all five GNSS observation cycles. External comparison of GNSS determinations with precise geometric levelling was performed for Cycles 3–5. Cycles 1–2, in which levelling was not performed, were used only in the analysis of the GNSS observation time series and were not included in the calculation of external accuracy indicators.

2.5. The 3 × 3 GNSS Reprocessing Scheme

Observations were performed using geodetic dual-frequency eSurvey E300 Pro receivers (Shanghai e-Compass Science & Technology Co., Ltd., Shanghai, China; https://www.esurvey-gnss.com/product/gnss/integrated-gnss-systems/E300-Pro, accessed on 7 November 2026) with forced antenna centring; rover data were recorded at 10 s intervals. All available 10 s epochs were used in processing. The original observations were converted to RINEX 3.02 format using the StaticToRinex converter supplied with the eSurvey E300 Pro GNSS receiver (Shanghai e-Compass Science & Technology Co., Ltd., Shanghai, China). The integrated ESVE300PRO_E31 antenna was used in all observations. According to the official NGS field calibration NGSRA_2440, the North/East/Up phase-centre offset (PCO) components are 1.7/1.6/70.2 mm for G01 (L1) and 0.7/0.6/63.1 mm for G02 (L2); the corresponding no-azimuth phase-centre variations (PCVs) over the zenith-angle range 0–80° reach 5.9 and 3.9 mm. The converter reduced the measured antenna heights to the phase centre and recorded this in a comment in the RINEX header. No additional user-defined phase-centre corrections were entered during post-processing.

A single GPS + GLONASS + Galileo combination was used; separate solutions by satellite constellation were not evaluated because the objective of the study was to compare the effects of the specified reference configurations and observation durations on GNSS height accuracy. The same GPS + GLONASS + Galileo constellation combination was used for all cycles and experimental configurations, ensuring comparability of the results. Changing the constellation composition would have introduced an additional factor and would not have allowed its influence to be unambiguously separated from the differences between session durations and the specified reference configurations. A comparative assessment of individual constellations requires a separate factorial experiment and was beyond the scope of this study. For each point, nested intervals of 15, 30,

and 60 min with the same start time were formed from the common record. Each interval was reprocessed for three predefined nested reference configurations: Burovaya; Burovaya + Poselkovyi; Burovaya + Poselkovyi + 5784. The specified reference configurations were compared as they were sequentially expanded: Burovaya; Burovaya-Poselkovyi; Burovaya-Poselkovyi-5784. The same rover observations and identical time intervals were used for all three configurations, enabling paired comparison of the three tested schemes under the conditions of the study site. The matrix of nine conditions is presented in Table 3.

Table 3. Reprocessing scheme for the common rover records, 3 × 3.

Configuration Designation	Reference Points	15 min	30 min	60 min
1	Burovaya	1 × 15	1 × 30	1 × 60
2	Burovaya + Poselkovyi	2 × 15	2 × 30	2 × 60
3	Burovaya + Poselkovyi + 5784	3 × 15	3 × 30	3 × 60

2.6. Establishment of the Reference Framework and GNSS Processing

Relative static processing was performed using Leica Geo Office (LGO, version 8.4; Leica Geosystems AG, Heerbrugg, Switzerland; https://leica-geosystems.com/rugbycl/archive-data/software/leica-geo-office, accessed on 7 November 2026): a separate project was created for each cycle and included all intervals and reference configurations for that cycle. The reference stations and baselines for each experimental configuration were specified manually; automatic segmentation of the common record into software-recognised sessions was not applied. The elevation mask was 10°. The maximum baseline length at the study site did not exceed 3.7 km. Broadcast ephemerides were used for all solutions: for such short baselines in the relative phase method, residual orbital errors are virtually identical at the reference station and rover and do not materially affect the observation differences. The same ephemeris type was used for all cycles and configurations. For all baseline solutions, the constellations and frequencies used were recorded, while ambiguity-resolution status was checked using the Ambiguity Status and Solution type fields.

A separate project was created for each cycle and included all specified intervals and reference configurations for the corresponding cycle.

In the strategy settings, frequency selection was set to automatic; ambiguity fixing was permitted for distances up to 80 km, the minimum duration for a static float solution was 300 s, and the Sampling rate parameter was set to Use all, meaning that all available epochs at the actual 10 s interval were used. The Saastamoinen tropospheric model was applied; ionospheric delay was handled automatically by the software. With a maximum baseline length of 3.7 km and simultaneous relative observations, ionospheric effects on the signals at the reference station and rover are highly correlated and are largely compensated when observation differences are formed. Therefore, a separate investigation of the influence of the ionospheric model and activity level was beyond the scope of this study. Stochastic modelling of ionospheric effects was enabled with a baseline-length threshold of 8 km. Because all investigated baselines did not exceed 3.7 km, this mode was not activated during processing.

The same processing models and parameters were applied under all nine experimental conditions; only the specified reference configuration and the duration of the

processed interval were varied. Quality control included checking the solution type and phase-ambiguity status, PDOP, the formal standard error of height for each baseline solution, and the consistency of multiple determinations of the same point. PDOP was used as the comparable overall indicator of the geometry of the combined GPS + GLONASS + Galileo solution. Representative indicators of satellite geometry and formal accuracy by cycle and session duration are presented in Table 4.

Table 4. Representative indicators of satellite geometry and formal accuracy of the baseline solutions for Rp-1…Rp-12.

Cycle	Duration, min	Median PDOP Interval (Overall Range)	SD(H), Median (Range), mm
1	15	1.70–2.00 (1.30–2.30)	0.8 (0.3–1.4)
1	30	1.50–2.10 (1.30–2.30)	0.6 (0.3–1.4)
1	60	1.50–2.20 (1.30–5.00)	0.4 (0.2–1.0)
2	15	1.60–2.00 (1.50–2.40)	0.8 (0.4–1.7)
2	30	1.50–2.10 (1.50–4.00)	0.6 (0.3–1.0)
2	60	1.50–2.20 (1.30–4.20)	0.4 (0.2–0.8)
3	15	1.70–1.90 (1.40–2.40)	0.8 (0.3–1.7)
3	30	1.70–2.00 (1.40–2.40)	0.6 (0.3–1.2)
3	60	1.60–2.20 (1.40–2.40)	0.5 (0.2–0.8)
4	15	1.70–2.00 (1.40–2.70)	0.8 (0.3–1.4)
4	30	1.70–2.10 (1.40–2.60)	0.6 (0.2–1.0)
4	60	1.60–2.25 (1.30–3.30)	0.4 (0.2–0.7)
5	15	1.70–2.15 (1.50–3.30)	0.8 (0.3–1.0)
5	30	1.60–2.15 (1.30–3.30)	0.6 (0.2–0.8)
5	60	1.50–2.30 (1.30–3.30)	0.4 (0.1–0.5)

Note: The statistics were calculated for the baseline solutions included in the analysis. PDOP is reported as the median $PDOP_{min}$–$PDOP_{max}$ interval, with the overall range in parentheses. SD(H) is the formal standard error of height for an individual baseline solution.

The reference framework was established in each cycle before the comparative analysis of the short rover sessions. At each stage, the reference points and corresponding baselines were assigned manually. Burovaya served as the primary reference station. In the next stage, the coordinates of Poselkovyi were determined relative to Burovaya, after which the coordinates of 5784 were determined using Burovaya and Poselkovyi as reference points. The full available intervals of simultaneous static observations, ranging from 5 to 18 h depending on the station and cycle, were used to determine the coordinates of the secondary reference stations. Baseline solutions with fixed phase ambiguities were included in the processing. Multi-baseline relative processing was applied, followed by weighted combination of the individual coordinate solutions. A separate Measured-class coordinate solution was generated for each specified baseline. Where several acceptable determinations of one station were available, Leica Geo Office 8.4 generated the final coordinates of the Averaged class using the Weighted method, taking account of the formal standard deviations of the individual solutions. Solutions with smaller standard deviations were assigned greater weights. The resulting reference-station coordinates were fixed before the 15, 30, and 60 min rover intervals were processed and were not re-determined separately for each of the nine configurations compared.

2.7. Local Conversion of Ellipsoidal Heights to the Normal-Height System

No global or regional geoid or quasigeoid model was applied in this study. GNSS results were transformed from WGS 84 to the local coordinate reference frame and the Baltic height reference frame by means of a local transformation with a planar approximation of the height component, established from four common GNSS/levelling points. This method was applied because the transformation parameters between WGS 84 and the local coordinate reference frame were unknown. The original geodetic coordinates in WGS 84 were known for Burovaya; the coordinates of the remaining common points were determined relative to it using static GNSS observations. The normal heights of the common points were obtained by precise geometric levelling and were used to realise the Baltic height reference frame. The height component of the local transformation was determined by a planar approximation of the discrepancies between ellipsoidal and normal heights at the common points. Thus, the transformed GNSS heights are normal heights referred to the Baltic height reference frame and were not obtained by applying a global or regional geoid or quasigeoid model. The type of result is inherited from the source normal heights of these points and the adopted reductions, rather than from the name of the software-interface mode [25,26].

Within the unified local transformation, the horizontal component was implemented using a two-dimensional Helmert transformation, and the height component was implemented using a planar approximation of corrections determined from four common GNSS/levelling points.

A three-dimensional seven-parameter Helmert transformation was not applied because, for its correct determination, the common points must be represented in two comparable three-dimensional geocentric coordinate reference frames. Local grid coordinates and normal heights were available at the site; however, the geodetic parameters of the local coordinate reference frame required to establish the target three-dimensional coordinates had not been documented. Furthermore, a seven-parameter transformation relates spatial coordinate reference frames but does not, by itself, provide a conversion from GNSS ellipsoidal heights to normal heights. Such a conversion would require a height-anomaly (quasigeoid) model consistent with the Baltic height reference frame; no such high-accuracy local model was applied for the study area. Therefore, a unified local transformation established from four common GNSS/levelling points was applied: the horizontal component was defined by a two-dimensional Helmert transformation, and the height component by a planar approximation of the differences between ellipsoidal and normal heights.

The height component was represented by a local correction plane with a constant term and two slopes with respect to the grid coordinates. Because the controlling heights were the normal heights of the common points in the Baltic height reference frame, the transformed GNSS heights belong to the same height reference frame. This avoids direct comparison of ellipsoidal and normal heights and preserves the distinction among normal, orthometric, and ellipsoidal heights [26].

The local transformation with a planar approximation of the height component was determined from four common GNSS/levelling points: Burovaya, Poselkovyi, 5784, and 4735. The ellipsoidal heights of these points were taken from the previously established and fixed coordinate solution, while their normal heights were obtained by precise geometric levelling. The constant term and two slopes of the local correction plane were determined from the differences between the normal and ellipsoidal heights. The coordinates of the four common points and the transformation parameters were fixed before the comparative processing of the nine experimental configurations; the same transformation was applied to all configurations without re-estimating its parameters.

Benchmarks Rp-1…Rp-12 were not used to determine the transformation parameters.

The transformation realised using Cycle 5 data was used in the primary analysis; it was selected on the basis of the best achieved levelling-convergence indicator before the external GNSS–levelling metrics were calculated. The parameters of the selected Cycle 5 transformation were fixed and applied identically to all five GNSS cycles and all nine configurations used to determine the heights of Rp-1…Rp-12. For the controlled Cycles 3–5, the sensitivity of the results to the source cycle used to realise the transformation was evaluated using transformations established from the data for Cycles 3, 4, and 5. The transformation parameters derived from Cycle 5 data and the corresponding internal accuracy indicators are presented in Table 5.

Table 5. Transformation parameters derived from Cycle 5 data and internal indicators.

Component	Parameter	Value	Purpose/Internal Characteristic
Input data	Common GNSS/levelling points	Burovaya; Poselkovyi; 5784; 4735 (n = 4)	Points used to determine the transformation
Horizontal	Method	Two-dimensional Helmert transformation	Linkage of WGS 84 to the local grid coordinate reference frame
Horizontal	A posteriori sigma	0.0045 m	Internal agreement of the horizontal component
Height	Model	Mean approximating plane	Tie to the Baltic height reference frame
Height	Slope along X	−0.00001789	Dimensionless correction-surface parameter
Height	Slope along Y	+0.00000719	Dimensionless correction-surface parameter
Height	Constant term	29.4999 m	Overall height level of the correction surface
Height	A posteriori RMSE of the height-transformation residuals, m_{tr}	0.0071 m	Internal agreement at the common points
Height	dH residuals	Burovaya −0.6; Poselkovyi +3.6; 5784 +2.5; 4735 −5.5 mm	Residuals at the four common points

The two-dimensional Helmert transformation relates the local grid coordinate reference frame to WGS 84, while the three parameters of the height-correction surface—two slopes and a constant term—provide conversion of ellipsoidal heights to normal heights in the Baltic height reference frame. The a posteriori RMSE and the residuals of the height component at the common points are internal characteristics of the agreement

and are not interpreted as ground-surface displacements. The designation 'dH residuals' in Table 5 refers to the components of the height-residual vector $\mathbf{v}_H$ used in the equation below.

The a posteriori RMSE of the height-transformation residuals was determined using the following equation:

$$m_{tr} = \sqrt{\frac{\mathbf{v}_H^T \mathbf{P} \mathbf{v}_H}{n-u}}$$

where $\mathbf{v}_H$ is the vector of height residuals at the common points; $\mathbf{P}$ is the weight matrix; $n = 4$ is the number of common points; and $u = 3$ is the number of parameters of the correction plane. For equal weights, $\mathbf{P} = \mathbf{I}$ and $n - u = 1$. For residuals of −5.5, +2.5, −0.6, and +3.6 mm, m_{tr} = 7.1 mm = 0.0071 m. This is an internal goodness-of-fit indicator with one degree of freedom, rather than an external accuracy estimate of the transformed GNSS heights.

For the local transformations with a planar approximation of the height component established from the data for Cycles 3, 4, and 5, m_{tr} was 5.9, 3.9, and 7.1 mm, respectively, while $\max|\mathbf{v}_H|$ was 4.6, 3.0, and 5.5 mm. The smallest internal discrepancy was obtained for Cycle 4. Cycle 5 was selected not on the basis of the minimum m_{tr}, but before the external metrics were calculated, using the minimum q_c value for the levelling routes. These indicators characterise different stages of the measurement chain.

The sensitivity analysis was performed by reprocessing all nine configurations using transformations established separately from the data for Cycles 3, 4, and 5. In each realisation, the ellipsoidal heights of the four common points were taken from the previously established coordinate solution for the corresponding cycle, while their normal heights were taken from precise geometric levelling in the same cycle. All three versions were applied to the same set of observations from Cycles 3–5 and were used for sensitivity analysis rather than as independent samples. The external metrics were calculated separately for Cycles 3–5 for each transformation version. Changing the transformation mainly altered the common height level: relative to the Cycle 5 transformation, the mean shifts $T_3 - T_5$ and $T_4 - T_5$ were −5.7 and −1.1 mm, with spatial SD values of approximately 0.8 and 0.4 mm, respectively. The tested three-reference configuration retained a lower RMSE than the corresponding one- and two-reference configurations in all 27 descriptive cells of the sensitivity analysis. Thus, the ranking of the tested reference configurations was retained when the source cycle used to establish the transformation was changed. The sensitivity analysis assesses the influence of the source cycle used to realise the transformation on the external metrics. The planar approximation of the height component is sensitive to the quality of the source normal heights at the common points; one fixed Cycle 5 transformation was retained for the inter-cycle analysis without re-fitting it at each epoch.

2.8. High-Precision Geometric Levelling

Vertical control was performed using a Leica LS15 digital level (Leica Geosystems AG, Heerbrugg, Switzerland; https://leica-geosystems.com/products/levels/digital-levels/leica-ls15-and-ls10, accessed on 7 November 2026) with a stated accuracy of ±0.3 mm per 1 km of double-run levelling and bar-coded invar staffs. In Cycles 3–5, high-precision geometric levelling was conducted along two closed and two control routes using an unchanged network layout. Corrections for the control misclosures were distributed with equal weights among the measured height differences of the corresponding route. The resulting normal heights were used for external comparison with the GNSS results

[27,28].

The levelling routes and their lengths were as follows: (1) Burovaya → 4735 → Poselkovyi → Burovaya—6.47–6.50 km; (2) 4735 → Rp-4 → Rp-8 → Rp-12 → Rp-11 → Rp-7 → Rp-1 → Rp-2 → Rp-5 → Rp-10 → Rp-9 → 4735—6.10 km; (3) 4735 → Rp-3 → Rp-6 → Rp-7—1.80 km; and (4) 5784 → Rp-11—0.70 km. Point 4735 is shown in the route profiles as the starting or closing point but was not included in the calculation of the external metrics for Rp-1…Rp-12.

The actual control misclosures of the four routes were +0.9, +7.6, −0.8, and +1.0 mm in Cycle 3; +5.0, +4.4, +0.0, and −0.4 mm in Cycle 4; and +2.1, +0.1, −0.1, and +0.2 mm in Cycle 5. All values satisfied the adopted verification condition $|f_j| \leq 5\sqrt{L}$ mm, where f_j is the misclosure of route j and L_j is its length in kilometres, . The following descriptive indicator was used to compare the achieved convergence of the cycles: The coefficient 5 mm/√km was adopted from the national Instruction on Levelling [27], in which $5\sqrt{L}$ mm is the allowable route-misclosure criterion for second-order levelling; it was used here as a pre-defined acceptance criterion and was not estimated from the observations.

$$q_c = \sqrt{\frac{1}{m}\sum_{j=1}^{m}\frac{f_j^2}{L_j}}$$

for $m = 4$ routes. The resulting q_c values were 1.7, 1.3, and 0.4 mm/√km for Cycles 3–5, respectively. The q_c indicator characterises the internal convergence of the routes and does not replace a full covariance-based uncertainty assessment. Levelling and GNSS were performed during overlapping periods: 24–27 and 25–27 April 2025; 17–20 and 20–21 July 2025; and 1–3 and 3–4 May 2026, respectively.

2.9. External Comparison and Interpretation of Inter-Cycle Changes

The high-precision levelling results were used as a more accurate external method of comparison, but not as error-free true values. Therefore, the difference between the GNSS and levelling heights characterises the agreement of the entire measurement chain, comprising the GNSS observations, local transformation, and levelling, rather than the error of GNSS alone.

Changes in the GNSS height of each point in Cycles 2–5 were calculated relative to Cycle 1. For the inter-method comparison, GNSS and levelling changes in Cycles 4 and 5 were calculated relative to Cycle 3:

$$\Delta H_{i,4-3}^{\mathrm{GNSS}} = H_{i,4}^{\mathrm{GNSS}} - H_{i,3}^{\mathrm{GNSS}}$$

$$\Delta H_{i,5-3}^{\mathrm{GNSS}} = H_{i,5}^{\mathrm{GNSS}} - H_{i,3}^{\mathrm{GNSS}}$$

$$\Delta H_{i,4-3}^{\mathrm{lev}} = H_{i,4}^{\mathrm{lev}} - H_{i,3}^{\mathrm{lev}}$$

$$\Delta H_{i,5-3}^{\mathrm{lev}} = H_{i,5}^{\mathrm{lev}} - H_{i,3}^{\mathrm{lev}}$$

A positive value indicates an increase in normal height in the later cycle. Inter-cycle changes were considered as dynamics rather than as an error of either method. Cycle 1 was adopted as the reference epoch for the five GNSS cycles; Cycle 3 was adopted as the

common reference epoch for the comparison of GNSS and levelling.

Inter-cycle changes were considered as normal-height dynamics and were evaluated in terms of magnitude, sign, repeatability, and spatial consistency along the route. Agreement in the direction of changes between GNSS and high-precision levelling was used to assess the reproducibility of the identified vertical dynamics.

2.10. Metrics and Statistical Analysis

The primary external-comparison dataset included Rp-1…Rp-12 in each of Cycles 3–5 (n = 12 for one configuration in one cycle). Point 4735 was not included in the statistical calculation because it was used to determine the local transformation. The following difference was calculated for each benchmark:

$$f_i = H^{\gamma}_{\mathrm{GNSS},i} - H^{\gamma}_{\mathrm{lev},i}$$

where γ denotes the monitoring cycle; a positive f_i indicates that the GNSS-derived height is higher than the levelling result. Five complementary indicators were used:

$$\mathrm{MD} = \frac{1}{n}\sum_{i=1}^{n} f_i$$

$$\mathrm{SD} = \sqrt{\frac{\sum_{i=1}^{n}(f_i - \mathrm{MD})^2}{n-1}}$$

$$\mathrm{MAE} = \frac{1}{n}\sum_{i=1}^{n} |f_i|$$

$$\mathrm{RMSE} = \sqrt{\frac{1}{n}\sum_{i=1}^{n} f_i^2}$$

$$|f|_{\max} = \max_{1 \le i \le n} |f_i|$$

MD characterises the mean signed difference between the normal heights obtained from GNSS and high-precision levelling. SD describes the dispersion after removal of MD; MAE is the mean absolute magnitude of the discrepancy; RMSE is more sensitive to large discrepancies; and max|f| indicates the worst individual case. RMSE is regarded as a measure of the inter-method agreement between GNSS and levelling after the local transformation, rather than as the standard deviation of a single GNSS measurement. All metrics were calculated separately for each cycle and each configuration.

The nine experimental configurations were compared separately for each of Cycles 3–5 using the same set of benchmarks. For each configuration, the mean signed difference (MD), standard deviation of the differences (SD), mean absolute difference (MAE), root mean square difference (RMSE), and maximum absolute difference were calculated; the effects of duration and reference configuration were evaluated by comparing these indicators within each cycle. Because the 15, 30, and 60 min intervals were formed from the same source records, and the configurations with one, two, and three reference stations were calculated from a common set of observations, the resulting configurations were treated as interrelated experimental configurations rather than as independent re-

peated measurements. Paired differences in absolute discrepancies were calculated for the same benchmark within the same controlled cycle (Cycles 3–5). Confidence intervals were estimated by resampling benchmarks while retaining the linked results from all three cycles and both configurations being compared (20,000 replicates). Paired differences were evaluated using an exact two-sided sign-flip permutation test applied to the benchmark-level means across cycles. For the selected 3 × 60 configuration, 95% bootstrap confidence intervals were also calculated separately for MAE and RMSE across the 12 benchmarks in each cycle. Calculations were performed in Python 3.12.14 with NumPy 2.3.5; a fixed initial state of the pseudorandom number generator was used for reproducibility.

The inter-cycle dynamics from GNSS and high-precision levelling were compared using changes in the normal heights of the same benchmarks and the route profiles ΔH_{GNSS} and ΔH_{lev}, taking into account the sign, magnitude, and spatial sequence of changes along the levelling lines. Agreement in the direction and spatial pattern of the changes was regarded as agreement between the observed trends, but not as equality of their amplitudes. A two-level rule was used for diagnostic screening: a network-wide signal required agreement in sign at no fewer than 75% of the benchmarks and a 95% bootstrap confidence interval for the median that excluded zero; a local signal was flagged when the centred residual exceeded three robust standard deviations estimated from the median absolute deviation (MAD). The recommended monitoring workflow is presented in Figure 4, and the investigated GNSS observation configurations are shown in Figure 5.

Figure 4 presents the recommended operational sequence rather than the chronology of the retrospective research processing. In the present study, after the Cycle 5 transformation had been determined, its parameters were fixed and applied retrospectively to all five GNSS cycles without epoch-specific fitting. The recommended workflow is divided into two technologically distinct phases. In Phase A, joint GNSS observations and high-precision levelling are used for the initial realisation of the local normal-height system, external verification, and fixation of the transformation parameters. Thereafter, in Phase B, repeated GNSS cycles are conducted independently using three reference stations, a 60 min duration, and a 10 s recording interval; the same fixed transformation is applied without refitting to levelling in each epoch. Activation of the diagnostic rule first triggers repeat GNSS observations using the unchanged network configuration. Control levelling is retained as a periodic external check and may be scheduled after confirmation of the signal in accordance with the monitoring programme. The workflow is shown in Figure 4, and the experimental configurations with one, two, and three reference stations are shown in Figure 5.

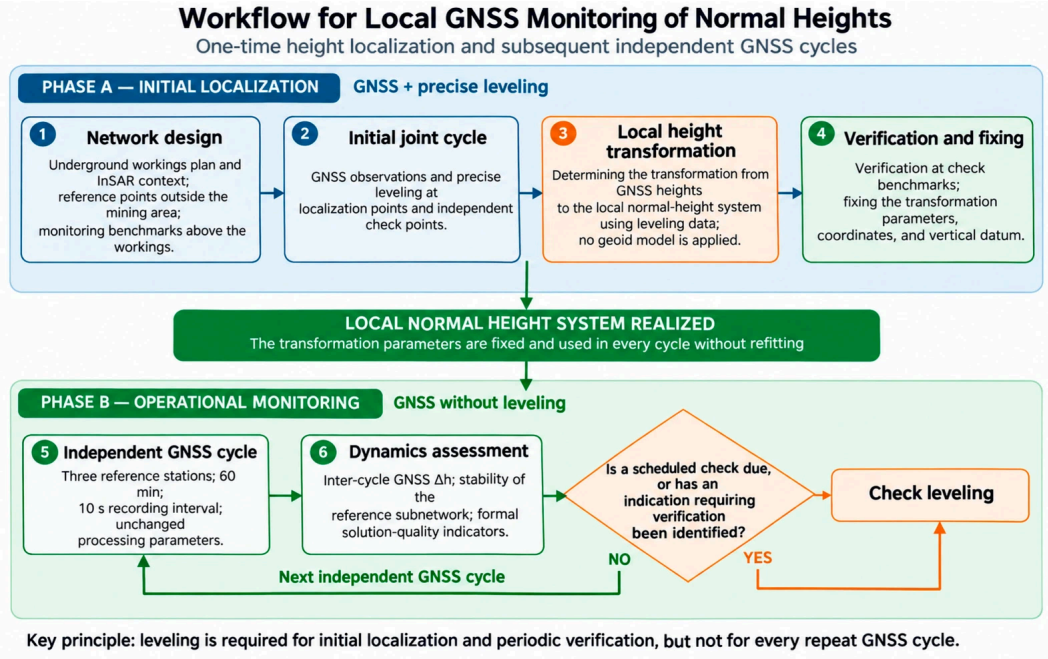


Figure 4. Recommended two-phase workflow for local GNSS height monitoring: initial localisation using joint GNSS and levelling data, followed by independent GNSS cycles using three reference stations × 60 min, with a fixed transformation and periodic or trigger-based levelling control.

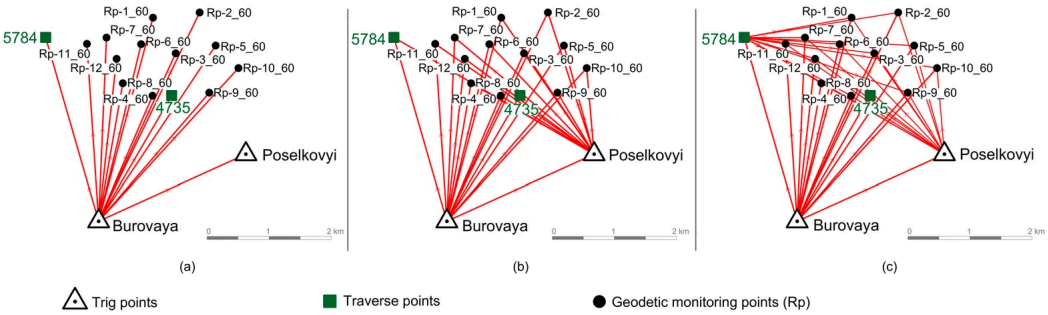


Figure 5. Static GNSS processing schemes associated with the technological sequence in Figure 4: (**a**) one reference station, Burovaya; (**b**) two reference stations, Burovaya and Poselkovyi; and (**c**) three reference stations, Burovaya, Poselkovyi, and 5784. Configuration (**c**), with a duration of 60 min and a recording interval of 10 s, was adopted as the preferred mode for the investigated site.

3. Results

The results are presented in three interrelated blocks: justification of the reference configuration, external comparison of the nine variants, and analysis of inter-cycle dynamics.

3.1. Spatial Justification of the Reference Configuration

According to the underground mine workings plan, the monitoring benchmarks are located above the mine-working corridors, while the three reference stations form an external triangle outside the surface projection of the shown workings. This separation precludes the use of a point located directly above the workings as a fixed datum and makes it possible to evaluate spatial changes within the object subnetwork relative to the external reference geometry.

Burovaya's location outside the mapped boundary of the underground mine workings was the primary spatial criterion for its selection. The magnitude of the later relative LOS velocity of the nearest persistent scatterer, +0.0 ± 1.9 mm/year, was smaller than its

corresponding formal 1σ uncertainty and was not statistically significant. This result supports the relative stability of Burovaya within the sensitivity of the method and the period covered by the InSAR data. The coordinates of Poselkovyi and 5784 were re-determined relative to Burovaya in each cycle before their inclusion in the reference configuration.

All four station-associated LOS-velocity intervals include zero relative to the original InSAR datum. Because the exact spatial reference and the inter-scatterer covariance are not fully documented, these relative velocities were not used to establish a statistically resolved ranking of station stability.

The hierarchy 'primary datum → two secondary stations re-determined in each cycle → monitoring benchmarks' is an essential component of the protocol [29]. It enables the use of a triangular multi-reference configuration without concealing the uncertainty of the auxiliary points behind an assumption of their permanent stability.

3.2. External Agreement of the Nine Variants in Cycles 3–5

The external evaluation was performed on Rp-1…Rp-12. All five metrics were calculated separately for each cycle and each of the nine configurations: the results for Cycle 3 are presented in Table 6, those for Cycle 4 in Table 7, and those for Cycle 5 in Table 8 (n = 12 for one configuration in one cycle).

Table 6. Discrepancies between GNSS- and levelling-derived normal heights in Cycle 3 at Rp-1…Rp-12; n = 12 for each configuration; units are mm.

Reference Stations	Time, min	MD	SD	MAE	RMSE	Max abs(f)
1	15	+9.1	10.6	11.8	13.6	23.4
1	30	+8.3	11.2	11.0	13.5	32.9
1	60	+5.0	8.7	7.6	9.7	18.7
2	15	+4.3	7.3	7.5	8.2	13.9
2	30	+4.9	6.2	6.7	7.7	14.1
2	60	+4.2	4.5	5.1	6.0	13.0
3	15	+4.4	3.0	4.8	5.2	8.8
3	30	+5.0	2.4	5.0	5.5	8.9
3	60	+3.6	3.0	3.9	4.6	7.8

Table 7. Discrepancies between GNSS- and levelling-derived normal heights in Cycle 4 at Rp-1…Rp-12; n = 12 for each configuration; units are mm.

Reference Stations	Time, min	MD	SD	MAE	RMSE	Max abs(f)
1	15	+1.5	12.1	9.3	11.7	24.5
1	30	−0.1	9.8	8.0	9.4	18.1
1	60	−1.5	7.2	6.2	7.1	14.8
2	15	−0.8	8.4	6.7	8.1	15.4
2	30	−0.8	6.5	4.7	6.2	12.7
2	60	−1.2	5.8	4.8	5.7	11.9
3	15	−1.9	3.1	2.9	3.5	7.3
3	30	−1.7	2.1	2.3	2.6	4.7
3	60	−2.0	3.0	3.0	3.5	7.3

Table 8. Discrepancies between GNSS- and levelling-derived normal heights in Cycle 5 at Rp-1…Rp-12; n = 12 for each configuration; units are mm.

Reference Stations	Time, min	MD	SD	MAE	RMSE	Max abs(f)
1	15	−0.7	6.6	5.6	6.4	10.3
1	30	−0.6	6.7	5.3	6.5	12.7
1	60	−0.7	6.5	5.0	6.3	11.1
2	15	−0.7	7.6	6.1	7.3	13.0
2	30	−0.4	5.9	4.7	5.6	12.9
2	60	−0.3	4.6	3.4	4.4	11.2
3	15	−0.3	3.8	3.1	3.6	7.1
3	30	−0.6	3.4	2.5	3.3	6.5
3	60	−0.5	2.5	1.9	2.4	5.1

The cycle-specific RMSE values for the 3 × 60 configuration were 4.6, 3.5, and 2.4 mm for Cycles 3, 4, and 5, respectively. Its MD changed from +3.6 mm in Cycle 3 to −2.0 and −0.5 mm in Cycles 4 and 5.

For the 3 × 60 configuration, the MAE [95% bootstrap confidence interval CI] and RMSE [95% bootstrap CI] were as follows: Cycle 3–3.9 [2.6, 5.3] and 4.6 [3.2, 5.7] mm; Cycle 4–3.0 [2.1, 4.1] and 3.5 [2.5, 4.6] mm; and Cycle 5–1.9 [1.1, 2.8] and 2.4 [1.5, 3.2] mm. These intervals characterise variation across the 12 control benchmarks but do not constitute a complete geodetic uncertainty budget [30].

Both benchmark groups are equipped with forced-centring mechanisms for the GNSS antenna; the comparison reflects differences in embedment depth and levelling-mark design. In a secondary analysis of the pooled Cycle 3–5 dataset, the existing Rp-1…Rp-6 had MAE = 3.0 mm and RMSE = 3.6 mm, whereas the new Rp-7…Rp-12 had values of 2.9 and 3.7 mm, respectively. The ‘new minus existing’ difference was −0.1 mm for MAE (95% CI −1.3 to +1.2 mm) and +0.1 mm for RMSE (95% CI −1.3 to +1.4 mm). Cluster bootstrap resampling by benchmark, jointly retaining all three cycles for each selected benchmark, was used for the confidence intervals of the group differences. No clear systematic difference between the groups was detected; the intervals included zero, while six benchmarks per group were insufficient to establish equivalence between the monument designs.

The effects of observation duration and the number of reference stations are presented separately for Cycle 3 in Figure 6, Cycle 4 in Figure 7, and Cycle 5 in Figure 8. For comparability, all three graphs were plotted at the same scale.

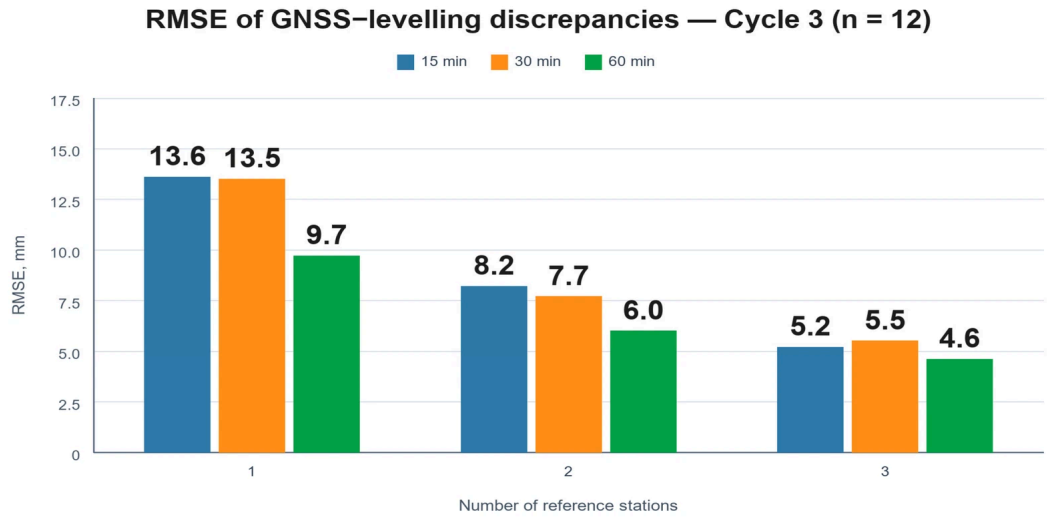


Figure 6. RMSE of discrepancies between GNSS- and levelling-derived normal heights in Cycle 3 with one, two, and three reference stations and durations of 15, 30, and 60 min; Rp-1…Rp-12, n = 12 for each configuration.

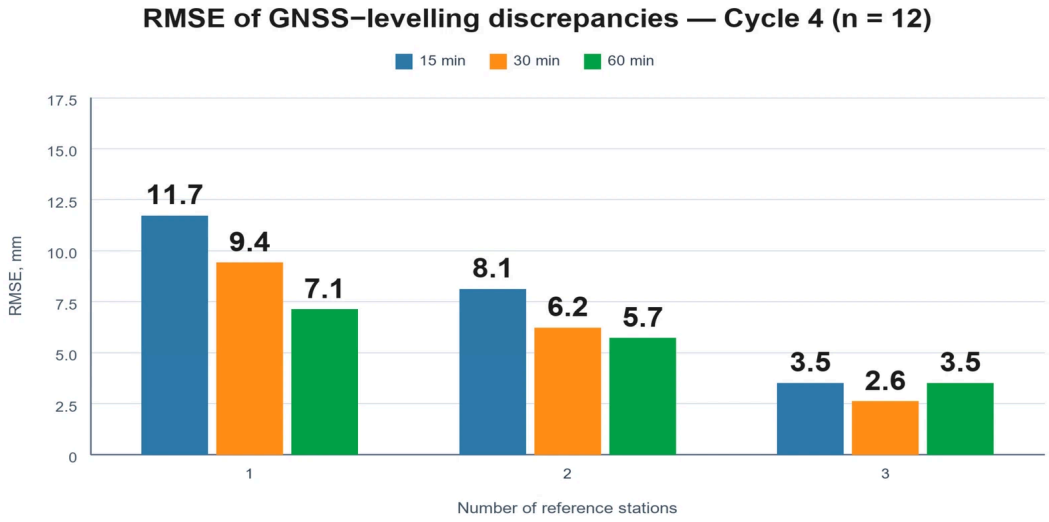


Figure 7. RMSE of discrepancies between GNSS- and levelling-derived normal heights in Cycle 4 with one, two, and three reference stations and durations of 15, 30, and 60 min; Rp-1…Rp-12, n = 12 for each configuration.

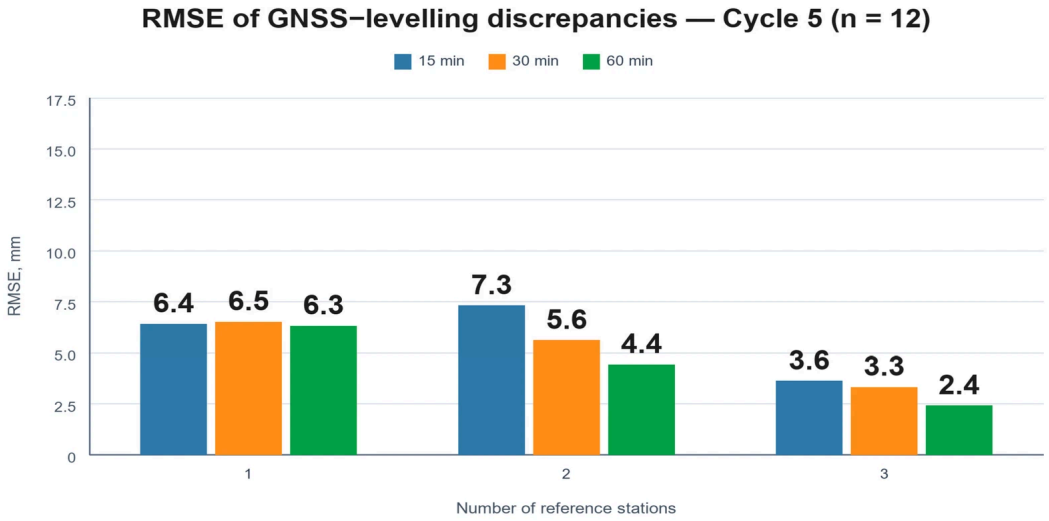


Figure 8. RMSE of discrepancies between GNSS- and levelling-derived normal heights in Cycle 5 with one, two, and three reference stations and durations of 15, 30, and 60 min; Rp-1…Rp-12, n = 12 for each configuration.

3.3. Justification for Selecting Three Reference Stations and 60 Min

Across all nine 'cycle × duration' combinations, the tested three-reference configuration Burovaya+Poselkovyi+5784 had a lower RMSE than the corresponding one- and two-reference configurations (Tables 6–8 and Figures 6–8). At a duration of 60 min, the RMSE values for configurations with three, two, and one reference stations were 4.6, 6.0, and 9.7 mm, respectively, in Cycle 3; 3.5, 5.7, and 7.1 mm in Cycle 4; and 2.4, 4.4, and 6.3 mm in Cycle 5. The recurrence of this result across all three cycles confirms the practical advantage of the complete three-reference configuration under the conditions of the investigated site.

In the three-reference configuration, the RMSE values at 15, 30, and 60 min were 5.3, 5.5, and 4.6 mm in Cycle 3; 3.5, 2.7, and 3.5 mm in Cycle 4; and 3.6, 3.3, and 2.4 mm in Cycle 5. The 60 min interval produced the minimum RMSE in Cycles 3 and 5, whereas the minimum value in Cycle 4 was obtained at 30 min. A 60 min interval was selected for a unified site-specific protocol: it showed consistently low cycle-specific discrepancies and contains a larger volume of phase observations than the nested 15 and 30 min intervals.

In the paired comparison of 36 'benchmark–cycle' combinations, changing from 30 to 60 min with three reference stations reduced the pooled RMSE by 0.4 mm; the 95% cluster-bootstrap CI for the RMSE difference was −0.9 to +0.1 mm. The mean paired difference in absolute discrepancies was ΔMAE = −0.315 mm (exact sign-flip p = 0.262), and the absolute discrepancy decreased in 21 of the 36 pairs. The observed advantage of 60 min over 30 min was small and statistically non-significant. At 60 min, the three-station configuration reduced the RMSE relative to two stations by 1.8 mm (95% CI −2.8 to −0.8 mm; ΔMAE = −1.511 mm; p = 0.0034) and relative to one station by 4.2 mm (95% CI −5.2 to −3.2 mm; ΔMAE = −3.341 mm; p = 0.0005). The p values relate to sign-flip tests of paired absolute discrepancies. The three-reference configuration therefore has paired statistical support for the tested geometry, whereas 60 min is regarded as a practical and robust working interval among those tested, rather than as a statistically demonstrated optimum.

Thus, the 3 × 60 configuration was adopted as the preferred site-specific protocol for further monitoring: it uses the complete spatial configuration, provided the lowest or near-lowest cycle-specific discrepancies, and remains substantially shorter than multi-hour static sessions. This conclusion applies to the investigated site and comparable compact networks with short baselines.

3.4. Inter-Cycle Dynamics from GNSS and Levelling

Cycles 1–2 had no external levelling control and were therefore not included in the inter-method comparison; their results were used only to describe the GNSS time series.

For Cycles 3–5, the dynamics obtained by the two methods were compared relative to a common reference epoch–Cycle 3. At Rp-1…Rp-12, the 3→4 transition has a negative direction according to both methods, while the subsequent 4→5 transition has a positive direction according to both methods. For the cumulative 3→5 transition, the spatial pattern is heterogeneous: the signs of ΔH_{GNSS} and ΔH_{lev} agree at 6 of the 12 benchmarks. These results describe dynamics rather than error; agreement in direction does not imply equality of amplitudes and, by itself, does not demonstrate statistically significant displacement of an individual benchmark [31,32].

For clarity, the results are presented separately for polygons 2 and 3, located above areas of underground mine workings. Figures 9 and 10 show the GNSS dynamics of Cycles 1–5 relative to Cycle 1 along polygons 2 and 3, respectively. Figures 11 and 12 compare changes from GNSS and high-precision levelling in Cycles 4 and 5 relative to Cycle 3 for the same routes. Solid lines with filled markers denote GNSS, dashed lines with open markers denote levelling, and colours distinguish the cycles. The same vertical scale was used for comparable pairs of figures.

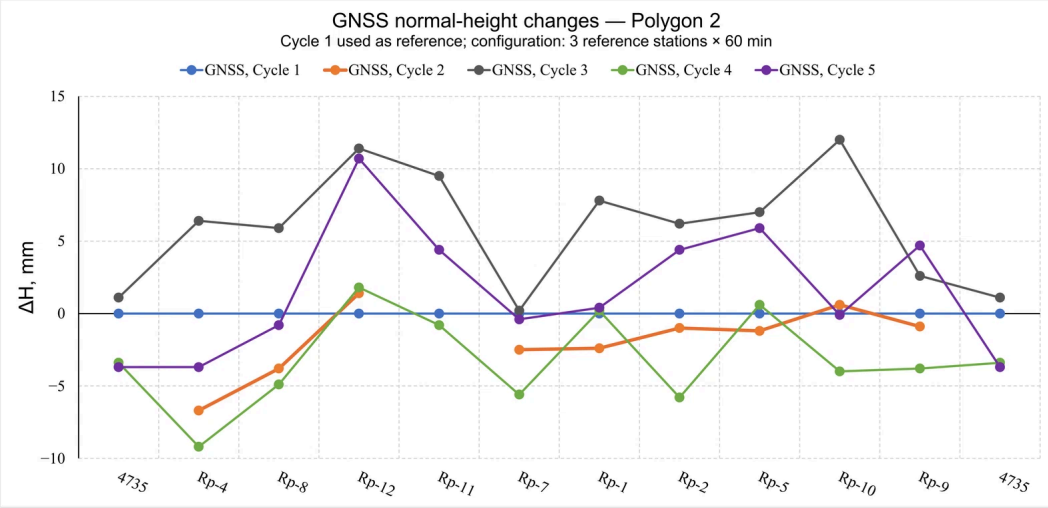


Figure 9. Dynamics of GNSS-derived normal heights relative to Cycle 1: polygon 2; configuration–three reference stations, 60 min.

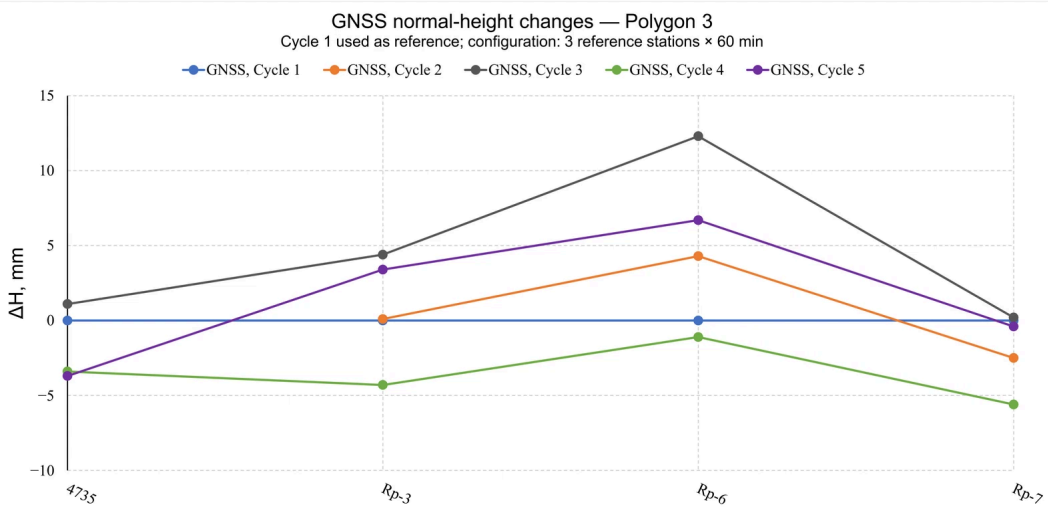


Figure 10. Dynamics of GNSS-derived normal heights relative to Cycle 1: polygon 3; configuration–three reference stations, 60 min.

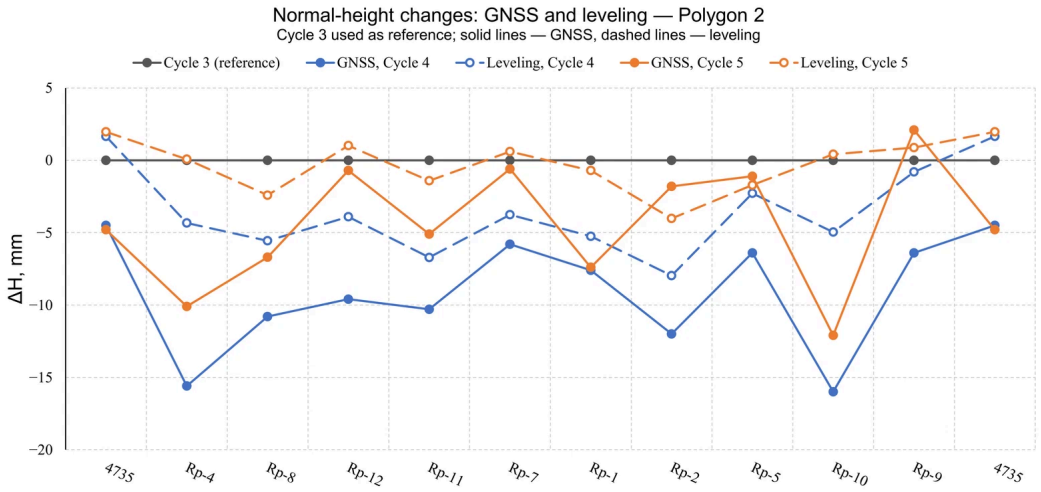


Figure 11. Comparison of inter-cycle dynamics from GNSS and high-precision levelling relative to Cycle 3: polygon 2.

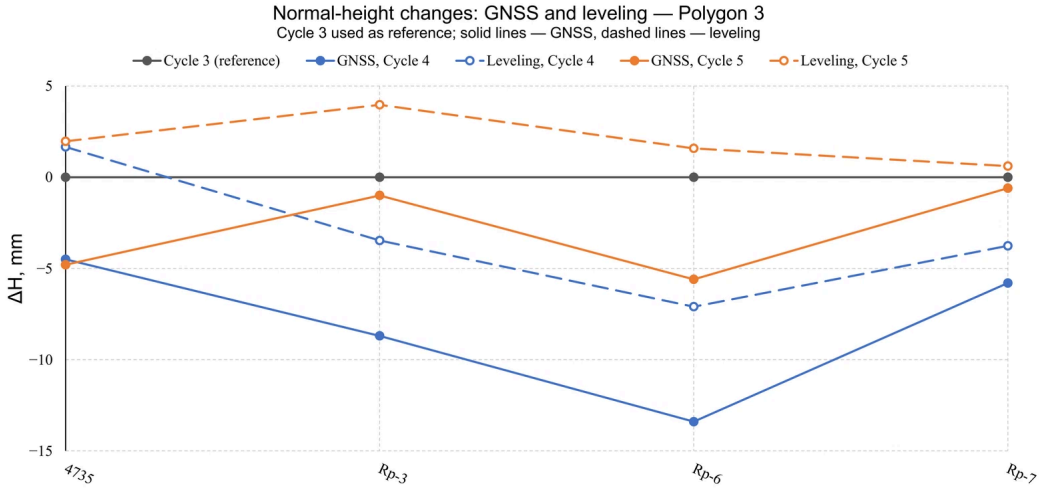


Figure 12. Comparison of inter-cycle dynamics from GNSS and high-precision levelling relative to Cycle 3: polygon 3.

According to Table 9, the mean q and RMSE(q) were −5.5 and 6.2 mm, respectively, for the 3→4 transition, and −4.0 and 5.9 mm for the 3→5 transition; after removal of the network-wide mean q, the centred RMSE values were 2.8 and 4.4 mm. For the 3→4 transition, the mean changes were −10.2 mm from GNSS and −4.7 mm from levelling, and the correlation coefficient for the pointwise changes was r = 0.546; for the cumulative 3→5 transition, the correlation coefficient was r = 0.127. For the adjacent 4→5 transition, the mean changes were +6.0 mm from GNSS and +4.5 mm from levelling; the RMSE of the pointwise differences was 3.5 mm, the correlation coefficient was r = 0.107, and the centred RMSE after removal of the network-wide mean was 3.2 mm. Under the proposed site-specific diagnostic screening rule, a network-wide signal was flagged when at least 75% of the benchmarks had the same sign of change and the 95% bootstrap CI for the median ΔH excluded zero. A local signal was assessed using the centred residual $e_i = \Delta H_i - \text{median}(\Delta H)$: a point was flagged if $|e_i| > 3 \times 1.4826 \times \text{MAD}(e)$. In the separate analysis of the sequential 3→4 and 4→5 transitions, the network-wide criterion was met: 12/12 benchmarks had the same sign, and the median GNSS changes were −10.0 mm (95% CI −12.7 to −7.0 mm) and +5.4 mm (95% CI 4.7 to 8.2 mm), respectively; the local criterion was not exceeded at any point. The proposed rule serves solely as a diagnostic

trigger for repeat GNSS observation and does not, in itself, demonstrate physical deformation or constitute a regulatory threshold; the operational response threshold is defined separately by the monitoring programme and safety requirements [33].

Table 9. Pointwise inter-cycle changes in normal height and differences $q = \Delta H_{GNSS} - \Delta H_{lev}$ for the 3 × 60 configuration using the Cycle 5 transformation; units are mm.

Point	ΔH_{lev} 3→4	ΔH_{GNSS} 3→4	q 3→4	ΔH_{lev} 3→5	ΔH_{GNSS} 3→5	q 3→5
Rp-1	−5.2	−7.6	−2.4	−0.7	−7.4	−6.7
Rp-2	−8.0	−12.0	−4.0	−4.0	−1.8	+2.2
Rp-3	−3.5	−8.7	−5.2	+4.0	−1.0	−5.0
Rp-4	−4.3	−15.6	−11.3	+0.1	−10.1	−10.2
Rp-5	−2.3	−6.4	−4.1	−1.7	−1.1	+0.6
Rp-6	−7.1	−13.4	−6.3	+1.6	−5.6	−7.2
Rp-7	−3.8	−5.8	−2.0	+0.6	−0.6	−1.2
Rp-8	−5.6	−10.8	−5.2	−2.4	−6.7	−4.3
Rp-9	−0.8	−6.4	−5.6	+0.9	+2.1	+1.2
Rp-10	−5.0	−16.0	−11.0	+0.4	−12.1	−12.5
Rp-11	−6.7	−10.3	−3.6	−1.4	−5.1	−3.7
Rp-12	−3.9	−9.6	−5.7	+1.0	−0.7	−1.7

4. Discussion

The results are interpreted below with due regard to the nested observations, sensitivity of the local transformation, and limits on the transferability of the resulting site-specific mode.

4.1. Scientific Novelty and Position Among Existing Studies

The study does not claim novelty for GNSS, InSAR, precise levelling, or multi-reference processing individually: such solutions have been published previously [1–4,6,7,10,11,14–20]. The scientific contribution lies in a closed-loop site-specific protocol: (i) the monitoring benchmarks are spatially linked to the surface projections of the mapped underground mine-working corridors; (ii) the external triangular reference subnetwork has an explicit hierarchy comprising one primary station and two stations re-determined in each cycle; (iii) nine conditions–1/2/3 stations × 15/30/60 min–are compared using the same rover records; (iv) the mode is selected using three cycles of external levelling control at benchmarks excluded from the determination of the local transformation; and (v) agreement in absolute heights is distinguished from agreement in inter-cycle changes. It is the combination of spatial design, a multi-campaign factorial comparison, and dynamic inter-method diagnostics that distinguishes this study from a one-time accuracy validation.

A similar three-reference configuration used by Baryła and Paziewski [6] involved eight-hour observations and precise levelling. Studies of observation duration [1–3,8,9] were conducted at different scales, with different monumentation types and criteria, whereas studies on InSAR-assisted placement of GNSS stations [17–19] do not address the selection of a short static session within a local normal-height system. The present study does not claim a universal new processing algorithm; its contribution is a reproducible experimental design and a quantitatively assessed and practically selected site-specific mode. A comparison with the most closely related studies is presented in Table 10.

Table 10. Position of the present study relative to the most closely related published approaches.

Source	Site and Configuration	Sessions	External Height Control	Distinction of the Present Study
[6]	Local mining network with three control points	8 h	Precise levelling	Similar geometry, but substantially longer sessions
[8]	Mining network approximately 3 × 8 km	Up to long-duration sessions; at least 12 h was recommended for height under the conditions investigated	Repeatability of GPS sessions, without external height control.	Confirms that a universal session duration is not transferable
[9]	15 CORS stations; deformation-network sensitivity	4, 6, 12, and 24 h	Without levelling comparison of heights	Relates duration to the minimum detectable displacement, rather than only to single-cycle RMSE
[19]	Underground coal mining; remote-sensing-based selection of GNSS stations	Continuous RTK context	Not a primary objective	Confirms that InSAR/remote-sensing screening for site selection is established
Present study	Site of 2.2 km^2; external reference and internal monitoring subnetworks; lines up to 3.7 km	15, 30, and 60 min from common records	Three cycles of precise levelling; 12 benchmarks excluded from transformation fitting	Nine paired comparable conditions, local normal heights, and comparison of inter-cycle dynamics

4.2. Possible Reasons for the Advantage of the Three-Reference Configuration

The advantage of the tested three-reference configuration, statistically confirmed using the adopted Cycle 5 transformation and descriptively retained across all three transformation variants, is likely related not only to the number of stations but also to the specific triangular geometry, additional baseline connections, and consistency checks on solutions obtained from different directions. Consequently, the conclusion is limited to the nested hierarchy Burovaya → Poselkovyi → 5784 and cannot be generalised to an arbitrary arrangement of three stations.

4.3. Justification of 60 min as a Practical and Robust Working Interval

The 60 min interval was retained as the preferred practical mode among those

tested: it was the longest interval considered, produced the lowest pooled RMSE with the adopted transformation, and maintained a consistently low worst cycle-specific result. The observed advantage of 60 min over 30 min was small and statistically non-significant. Therefore, 60 min is regarded as a practical and robust working interval among those tested, rather than as a statistically demonstrated optimum.

In the regulatory context, the geodetic observation programme applied at geodynamic monitoring sites in the Republic of Kazakhstan provides for longer sessions [34]. The investigated 60 min mode is shorter than that programme and is considered an experimental supplementary monitoring mode. The obtained result does not confirm regulatory equivalence and does not provide grounds for unilateral replacement of the established observation programme.

4.4. Interpretation of the Observed Inter-Cycle Signal

The single-cycle RMSE of 2.4 mm characterises the external agreement achieved between the configuration 'three reference stations, 60 min' and high-precision levelling in Cycle 5. In the analysis of inter-cycle dynamics, the direction of changes and the quantitative differences in their amplitudes along the levelling routes were compared. A change detected by GNSS is treated as a monitoring signal and is verified by a repeated GNSS observation using an unchanged network configuration; high-precision levelling serves as periodic external control of the height reference frame.

For the 3→4 and 4→5 transitions, the signs of the normal-height changes obtained by GNSS and high-precision levelling agreed at all 12 monitoring benchmarks. However, agreement in local amplitudes was limited: for the 3→4 transition, the correlation coefficient of pointwise changes was $r = 0.55$, and the RMSE of the differences in inter-cycle changes was 6.2 mm; for the 4→5 transition, the corresponding values were $r = 0.11$ and 3.5 mm. Consequently, the results confirm agreement in the overall direction of network dynamics, but not the identity of pointwise amplitudes or spatial patterns. This preserves the value of GNSS as an operational indicator of a network-wide inter-cycle signal.

Verification of the initial coordinates and heights of the reference stations before the inter-cycle analysis is a mandatory part of the protocol, because an error in an initial value can produce a network-wide shift.

4.5. Operational Role of GNSS Under Adverse Winter Conditions

Snow cover, strong winds, and limited periods of stable visibility increase the labour intensity of precise levelling and the risk of compromising the reproducibility of portable support placement. This does not make winter levelling methodologically impossible. In the present study, levelling control was absent in Cycles 1–2 owing to a combination of field and organisational reasons; only Cycle 2 occurred during winter. Therefore, the substantiated conclusion concerns the operational continuity of GNSS between full levelling cycles, rather than the impossibility of winter levelling or general practice at all mines.

The developed 3.2 m deep geodetic monument design provides reproducible forced centring of the GNSS antenna and is intended to reduce the influence of near-surface conditions on monument stability.

4.6. Practical Applicability and Scope of Use

The 3 × 60 configuration can be used as a site-specific mode for intermediate control of a compact network with short baselines, forced centring, and cycle-by-cycle re-determination of the secondary stations. The workflow comprises network design taking ac-

count of the mine-workings plan, subsequent spatio-temporal characterisation of the reference configuration using InSAR data, verification of the initial heights of the reference stations, one-hour GNSS observation, local conversion to normal heights, analysis of the network-wide and local components, and periodic precise levelling. This operational workflow complements the numerical geomechanical modelling previously conducted at the Vostochnaya-Saryoba deposit [35]. The patented monument design supports repeatable antenna installation and connection to a separate levelling mark, but it is not the principal source of accuracy or the main scientific novelty.

After the local height transformation has been established and the selected configuration verified, subsequent monitoring cycles can be performed independently using GNSS. A change detected simultaneously at several neighbouring benchmarks is verified by a repeated GNSS observation with the network configuration and processing parameters unchanged. High-precision levelling is applied periodically to control the stability of the height reference frame, rather than to provide mandatory confirmation of every GNSS result.

5. Conclusions

A site-specific monitoring configuration was developed and repeatedly tested in which the external triangular reference subnetwork is spatially separated from the surface projection of the mapped underground workings, while twelve monitoring benchmarks are located above the mining areas. The magnitude of the later relative LOS velocity of the persistent scatterer nearest to Burovaya was smaller than its corresponding formal 1σ uncertainty and was not statistically significant. This result supports the relative stability of Burovaya within the sensitivity of the method and the period covered by the InSAR data.

For the Burovaya+Poselkovyi+5784/60 min configuration, the RMSE of the external differences was 4.6, 3.5, and 2.4 mm in Cycles 3–5, respectively. At 60 min, the tested three-reference configuration had a statistically confirmed advantage over the one- and two-reference configurations; however, the advantage of 60 min over 30 min was small and statistically non-significant. Therefore, 60 min is regarded as a practical and robust working interval among those tested, rather than as a statistically demonstrated optimum.

Sensitivity analysis using three transformation versions, applied to the same dataset from Cycles 3–5, showed that the choice of source levelling cycle primarily affects the common height level and the external differences. In all 27 descriptive cells, the three-reference configuration retained a lower RMSE than the one- and two-reference configurations; these cells were not treated as independent samples. The a posteriori standard deviation of the height residuals, m_{tr}, was 5.9, 3.9, and 7.1 mm for transformations derived from Cycles 3, 4, and 5, respectively. Cycle 5 was selected not by minimising m_{tr}, but a priori on the basis of the smallest q_c = 0.4 mm/√km. The parameters of the selected transformation were fixed for all epochs without cycle-specific fitting.

For the 3→4 and 4→5 transitions, GNSS and levelling showed the same overall direction at all 12 benchmarks, but agreement in pointwise amplitudes was weaker. The proposed configuration is therefore suitable for operational detection of a network-wide inter-cycle signal followed by repeat GNSS control; transfer of the quantitative performance characteristics to other networks requires verification for comparable baseline lengths, geometry, and monumentation.

Supplementary Materials: The following supporting information can be downloaded at: https://www.mdpi.com/article/10.3390/app162211221/s1, The following electronic spreadsheets accompany the article: 1_Data S1–S5_with transformation data_3 cycles—GNSS observation results, precise

levelling results, and accuracy assessment for Cycles 1–5 (XLSX), using transformation parameters determined from Cycle 3; 2_Data S1–S5_with transformation data_4 cycles—GNSS observation results, precise levelling results, and accuracy assessment for Cycles 1–5 (XLSX), using transformation parameters determined from Cycle 4; 3_Data S1–S5_with transformation data_5 cycles—GNSS observation results, precise levelling results, and accuracy assessment for Cycles 1–5 (XLSX), using transformation parameters determined from Cycle 5.

Author Contributions: Project administration, G.M. (Guldana Meirambek); supervision, G.M. (Guldana Meirambek); investigation, Z.S., K.R., M.N.; formal analysis, Z.S., E.B., D.K., S.S., S.A., G.M. (Gulmira Madimarova) and A.N.; writing—original draft, Z.S.; writing—review and editing, all authors. All authors have read and agreed to the published version of the manuscript.

Funding: This research was funded by the Science Committee of the Ministry of Science and Higher Education of the Republic of Kazakhstan, grant number AP23489269, under the project "Geotechnical Monitoring of Geodynamic State of Geological and Structural Environment of Rock Mass during Subsoil Development to Ensure Industrial Reliability".

Institutional Review Board Statement: Not applicable: the study did not involve humans, animals, biological materials, or personal data.

Informed Consent Statement: Not applicable: the study did not involve human participants or identifiable personal data.

Data Availability Statement: GNSS and precise levelling data for Cycles 1–5, including results obtained with transformations derived from Cycles 3, 4, and 5, are provided in Supplementary Data files S1–S3. The InSAR acquisition period, network statistics, processing parameters, selection criteria, and station results are reported in Section 2.2 and Table 1.

Conflicts of Interest: The authors declare no conflicts of interest.

Abbreviations

GNSS	Global Navigation Satellite System
GPS	Global Positioning System
GLONASS	Global Navigation Satellite System
InSAR	Interferometric Synthetic Aperture Radar
SAR	Synthetic Aperture Radar
LOS	Satellite Line of Sight
IW	Sentinel-1 Interferometric Wide Swath mode
VV	Vertical transmit and vertical receive radar polarisation
SRTM	Shuttle Radar Topography Mission digital elevation model
RINEX	Receiver Independent Exchange Format for GNSS data
PDOP	Position Dilution of Precision
MD	Mean Signed Difference
SD	Standard Deviation of Differences
SD(H)	Formal Standard Error of Height
MAE	Mean Absolute Difference
RMSE	Root Mean Square Difference
CI	Confidence Interval
WGS 84	World Geodetic System 1984
NOAA	US National Oceanic and Atmospheric Administration
NGS	US National Geodetic Survey

RTK	Real-Time Kinematic
CORS	Continuously Operating Reference Stations
L1/L2	L1 and L2 GNSS carrier frequencies
RS	Remote Sensing
Rp	Monitoring-Network Benchmark

References

1. Eckl, M.C.; Snay, R.A.; Soler, T.; Cline, M.W.; Mader, G.L. Accuracy of GPS-derived relative positions as a function of interstation distance and observing-session duration. *J. Geod.* **2001**, *75*, 633–640. [Google Scholar] [CrossRef]
2. Firuzabadi, D.; King, R.W. GPS precision as a function of session duration and reference frame using multi-point software. *GPS Solut.* **2012**, *16*, 191–196. [Google Scholar] [CrossRef]
3. Elaksher, A.; Ali, T.; Kamtchang, F.; Wegmann, C.; Guerrero, A. Performance analysis of multi-GNSS static and RTK techniques in estimating height differences. *Int. J. Digit. Earth* **2020**, *13*, 586–601. [Google Scholar] [CrossRef]
4. Wang, H.; Dai, W.; Yu, W. BDS/GPS multi-baseline relative positioning for deformation monitoring. *Remote Sens.* **2022**, *14*, 3884. [Google Scholar] [CrossRef]
5. Dawidowicz, K.; Baryła, R. GNSS antenna caused near-field interference effect in precise point positioning results. *Artif. Satell.* **2017**, *52*, 27–40. [Google Scholar] [CrossRef]
6. Baryła, R.; Paziewski, J. The concept of the GNSS control network densification with precise leveling for ground deformation monitoring. In Proceedings of the 9th International Conference Environmental Engineering, Vilnius, Lithuania, 22–23 May 2014. [Google Scholar] [CrossRef]
7. Baryła, R.; Paziewski, J.; Wielgosz, P.; Stępniak, K.; Krukowska, M. Accuracy assessment of the ground deformation monitoring with the use of GPS local network: Open pit mine Koźmin case study. *Acta Geodyn. Geomater.* **2014**, *11*, 317–324. [Google Scholar] [CrossRef]
8. Bazanowski, M.; Szostak-Chrzanowski, A.; Chrzanowski, A. Determination of GPS session duration in ground deformation surveys in mining areas. *Sustainability* **2019**, *11*, 6127. [Google Scholar] [CrossRef]
9. Erkoç, M.H.; Doğan, U.; Aydın, C. Observing-session duration optimization of GPS deformation networks using point-sensitivity ellipses. *Acta Geodyn. Geomater.* **2025**, *22*, 183–194. [Google Scholar] [CrossRef]
10. Abetov, A.; Katrenov, Z.; Kudaibergenova, S.; Kisseyeva, S. Integrated geodynamic monitoring and risk assessment of deformation processes at the Bozashy North oil and gas field. *News Natl. Acad. Sci. Repub. Kazakhstan Ser. Geol. Tech. Sci.* **2025**, *3*, 9–26. [Google Scholar] [CrossRef]
11. Tao, Q.; Liu, R.; Li, X.; Gao, T.; Chen, Y.; Xiao, Y.; He, H.; Wei, Y. A method for monitoring three dimensional surface deformation in mining areas combining SBAS-InSAR, GNSS and probability integral method. *Sci. Rep.* **2025**, *15*, 2853. [Google Scholar] [CrossRef] [PubMed]
12. Jiang, W.; Chen, Y.; Chen, Q.; Chen, H.; Pan, Y.; Liu, X.; Liu, T. High precision deformation monitoring with integrated GNSS and ground range observations in harsh environment. *Measurement* **2022**, *204*, 112179. [Google Scholar] [CrossRef]
13. Yang, J.; Tang, W.; Xuan, W.; Xi, R. Tight integration of GNSS and static level for high accuracy dilapidated house deformation monitoring. *Remote Sens.* **2022**, *14*, 2943. [Google Scholar] [CrossRef]
14. Béjar-Pizarro, M.; Guardiola-Albert, C.; García-Cárdenas, R.P.; Herrera, G.; Barra, A.; López Molina, A.; Tessitore, S.; Staller, A.; Ortega-Becerril, J.A.; García-García, R.P. Interpolation of GPS and geological data using InSAR deformation maps: Method and application to land subsidence in the Alto Guadalentín Aquifer (SE Spain). *Remote Sens.* **2016**, *8*, 965. [Google Scholar] [CrossRef]
15. Fuhrmann, T.; Caro Cuenca, M.; Knöpfler, A.; van Leijen, F.J.; Mayer, M.; Westerhaus, M.; Hanssen, R.F.; Heck, B. Estimation of small surface displacements in the Upper Rhine Graben area from a combined analysis of PS-InSAR, levelling and GNSS data. *Geophys. J. Int.* **2015**, *203*, 614–631. [Google Scholar] [CrossRef]
16. Kong, X.; Wang, X.; Chen, Z.; Huang, M. An uncertainty-weighted fusion method of PS-InSAR, GNSS, and leveling for millimeter-level deformation monitoring in sensitive observatory environments. *Measurement* **2026**, *268*, 120660. [Google Scholar] [CrossRef]
17. Mao, W.; Li, Z.; Wang, Z.; Li, P.; Zhu, Y.; Hou, J. GNSS ground deformation observation network optimization assisted using prior InSAR-derived ground surface deformation and multiscale iteration estimation. *Int. J. Digit. Earth* **2024**, *17*, 2329348. [Google Scholar] [CrossRef]

18. Xu, H.; Shu, B.; Zhang, Q.; Du, Y.; Zhang, J.; We, T.; Xiong, G.; Dai, X.; Wang, L. Site selection for landslide GNSS monitoring stations using InSAR and UAV photogrammetry with analytical hierarchy process. *Landslides* **2024**, *21*, 791–805. [Google Scholar] [CrossRef]
19. He, Y.; Yu, X.; Su, H.; Xie, Z.; Su, Q.; Sun, L.; Feng, P.; Lin, Z.; Su, R. A multi-source remote-sensing-assisted method for GNSS station site selection in underground coal-mining subsidence areas. *Sensors* **2026**, *26*, 5057. [Google Scholar] [CrossRef] [PubMed]
20. Nguyen, H.V.; Pham, K.C.; Nguyen, D.B.; Nguyen, L.Q. Application of the GNSS method in the monitoring of mine surface displacement: A systemic review. *Inż. Miner.* **2024**, *53*, 247–255. [Google Scholar] [CrossRef]
21. Yunjun, Z.; Fattahi, H.; Amelung, F. Small baseline InSAR time series analysis: Unwrapping error correction and noise reduction. *Comput. Geosci.* **2019**, *133*, 104331. [Google Scholar] [CrossRef]
22. MintPy Development Team. MintPy Documentation. Available online: https://mintpy.readthedocs.io/ (accessed on 23 October 2026).
23. MintPy Development Team. MintPy, Version 1.6.4. 25 July 2026. Available online: https://github.com/insarlab/MintPy/releases/tag/v1.6.4 (accessed on 23 October 2026). [Google Scholar]
24. Committee for Construction and Housing and Communal Services of the Republic of Kazakhstan. SP RK 2.04-01-2017 "Construction Climatology", as Amended 13 May 2025. Available online: https://new-shop.ksm.kz/egfntd/ntdgo/kds/ (accessed on 26 August 2026).
25. Yanalak, M.; Baykal, O. Transformation of ellipsoid heights to local leveling heights. *J. Surv. Eng.* **2001**, *127*, 90–103. [Google Scholar] [CrossRef]
26. Hofmann-Wellenhof, B.; Moritz, H. *Physical Geodesy*, 2nd ed.; Springer: Vienna, Austria, 2006; 403p. [Google Scholar] [CrossRef]
27. Minister of Digital Development, Innovations and Aerospace Industry of the Republic of Kazakhstan. Order of 16 March 2023 No. 94/NQ, Instruction on Leveling; Registered by the Ministry of Justice on 17 March 2023, No. 32090. Available online: https://adilet.zan.kz/rus/docs/V2300032090 (accessed on 22 August 2026).
28. Minister of Digital Development, Innovations and Aerospace Industry of the Republic of Kazakhstan. Order of 27 March 2023 No. 107/NQ, Instruction on the Creation and Development of State Geodetic, Leveling and Gravimetric Networks; Registered by the Ministry of Justice on 30 March 2023, No. 32167. Available online: https://adilet.zan.kz/rus/docs/V2300032167 (accessed on 23 August 2026).
29. Wang, D.; Huang, G.; Du, Y.; Zhang, Q.; Bai, Z.; Tian, J. Stability analysis of reference station and compensation for monitoring stations in GNSS landslide monitoring. *Satell. Navig.* **2023**, *4*, 29. [Google Scholar] [CrossRef]
30. Joint Committee for Guides in Metrology. *Evaluation of Measurement Data—Guide to the Expression of Uncertainty in Measurement*; JCGM 100:2008(E); JCGM: Sèvres, France, 2008. [Google Scholar] [CrossRef]
31. Prószyński, W.; Łapiński, S. Investigating support by minimal detectable displacement in confidence region determination and significance test of displacements. *J. Geod.* **2021**, *95*, 112. [Google Scholar] [CrossRef]
32. Savšek-Safić, S.; Ambrožič, T.; Stopar, B.; Turk, G. Determination of point displacements in the geodetic network. *J. Surv. Eng.* **2006**, *132*, 58–63. [Google Scholar] [CrossRef]
33. U.S. Army Corps of Engineers. *Structural Deformation Surveying*; Engineer Manual EM 1110-2-1009; Department of the Army: Washington, DC, USA, 2018. Available online: https://www.publications.usace.army.mil/portals/76/publications/engineermanuals/em_1110-2-1009.pdf (accessed on 23 August 2026).
34. Acting Minister of Digital Development, Innovations and Aerospace Industry of the Republic of Kazakhstan. Order of 11 January 2024 No. 13/NQ, Instruction on Geodetic Work at Geodynamic Polygons; Registered by the Ministry of Justice on 15 January 2024, No. 33906. Available online: https://adilet.zan.kz/rus/docs/V2400033906 (accessed on 23 August 2026).
35. Meirambek, G.; Nurpeissova, M.B.; Rysbekov, K.B.; Kirgizbaeva, D.M.; Soltabayeva, S.T.; Shakirov, Z.B.; Turumbetov, T.A.; Adilbekova, L.K. Numerical Modelling of Stress–Strain State During Combined Mining of Zhilandy Group of Deposits. *ES Energy Environ.* **2026**, *31*, 1909. [Google Scholar] [CrossRef]

Disclaimer/Publisher's Note: The statements, opinions and data contained in all publications are solely those of the individual author(s) and contributor(s) and not of MDPI and/or the editor(s). MDPI and/or the editor(s) disclaim responsibility for any injury to people or property resulting from any ideas, methods, instructions or products referred to in the content.